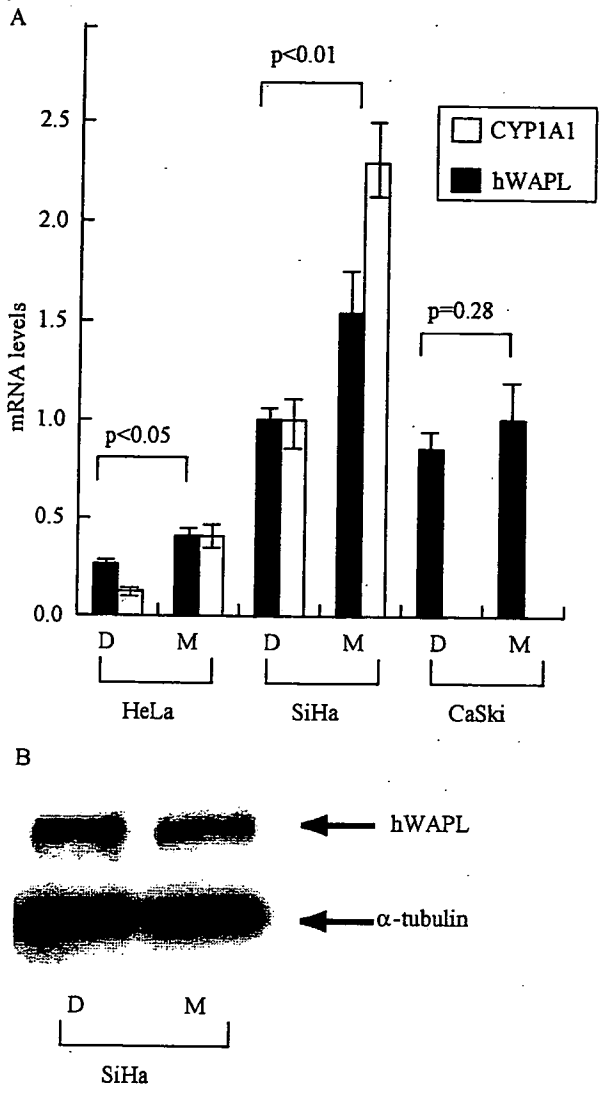

Fig. 1. Effects of 3-MC on *hWAPL* expression in the human cervical cancer-derived cell lines. D, DMSO alone; M, 3-MC. (A) HeLa, SiHa and CaSki cells were treated with 0.1% DMSO alone or 1 μM of 3-MC for 6 h. Then, the *hWAPL* and *CYP1A1* mRNA levels in the cells were evaluated by quantitative real time PCR analysis. Data were normalized to the mRNA levels of SiHa cells treated with DMSO alone that was arbitrarily set to 1 in the graphical presentation. *Bars, s.e.* (B) SiHa cells were treated with 0.1% DMSO alone or 1 μM 3MC for 6 h, and then the protein samples were prepared and subjected to western blotting analysis. α-tubulin was also shown as a loading control.

except for the 40 PCR cycles at 95 °C for 3 s and 68 °C for 30 s. Real Time PCR analysis for human *CYP1A1* mRNA and *hWAPL* hnRNA was also performed with the same PCR protocol. The nucleotide sequences of primers specific for human *CYP1A1* mRNA were previously described [11]. Primers specific for *hWAPL* hnRNA are 5′-GAGATTACACCACTGCACTCC-3′ and 5′-TTGCTCCCACTTACTATGGCC-3′. For mouse cDNAs, we used primers specific for the mouse homolog of *hWAPL* mRNA, 5′-ACCTGGTGGAGTATAGTGCCC-3′ and 5′-TGGCAGAGACACCCAAGAAGC-3′ (The nucleotide sequences were obtained from mKIAA0261 in Database), mouse β-*actin* mRNA, 5′-AGCCTTCCTTCTTGGGTATGG-3′ and 5′-CACTTGCGGTGCACGATGGAG-3′, and mouse *CYP1A1* mRNA, 5′-TTTGGTTTGGGCAAGCGA-3′ and 5′-GTCTAAGCCTGAAGATGC-3′. Reaction mixtures were denatured at 95 °C for 30 s then subjected to 40 PCR cycles at 95 °C for 3 s, 68 °C for 30 s, and 86 °C for 6 s for mouse *WAPL* mRNA, and at 95 °C for 3 s, 68 °C for 30 s, and 85 °C for 6 s for mouse β-*actin* and *CYP1A1* mRNAs, respectively. *hWAPL, mouse WAPL* and human and mouse *CYP1A1* mRNA levels and *hWAPL* hnRNA level were normalized to human and mouse β-*actin* signals, respectively. The absence of PCR products after the PCR on non-reverse-transcribed total RNA served as a routine check for contaminating genomic DNA. We performed the experiments to determine mRNA and hnRNA levels in triplicate.

The data were analyzed using Student's-*t* test, and $Ps < 0.05$ were considered to indicate significant differences.

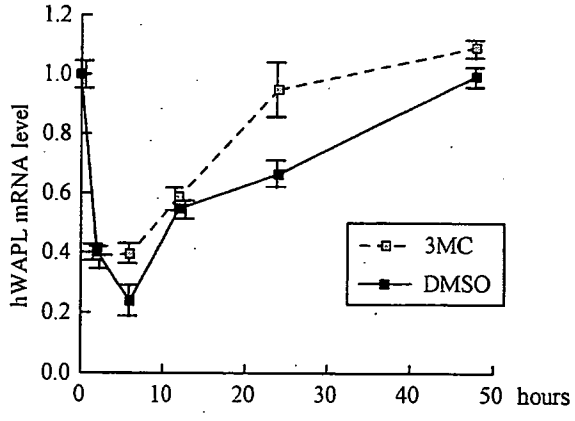

Fig. 2. Kinetics of *hWAPL* mRNA levels in SiHa cells at several time points after treatment with DMSO alone or 1 μM of 3-MC. The *hWAPL* mRNA levels in the cells were evaluated by quantitative real time PCR analysis. Data were normalized to the mRNA level at 0 h that was arbitrarily set to 1 in the graphical presentation. *Bars, s.e.*

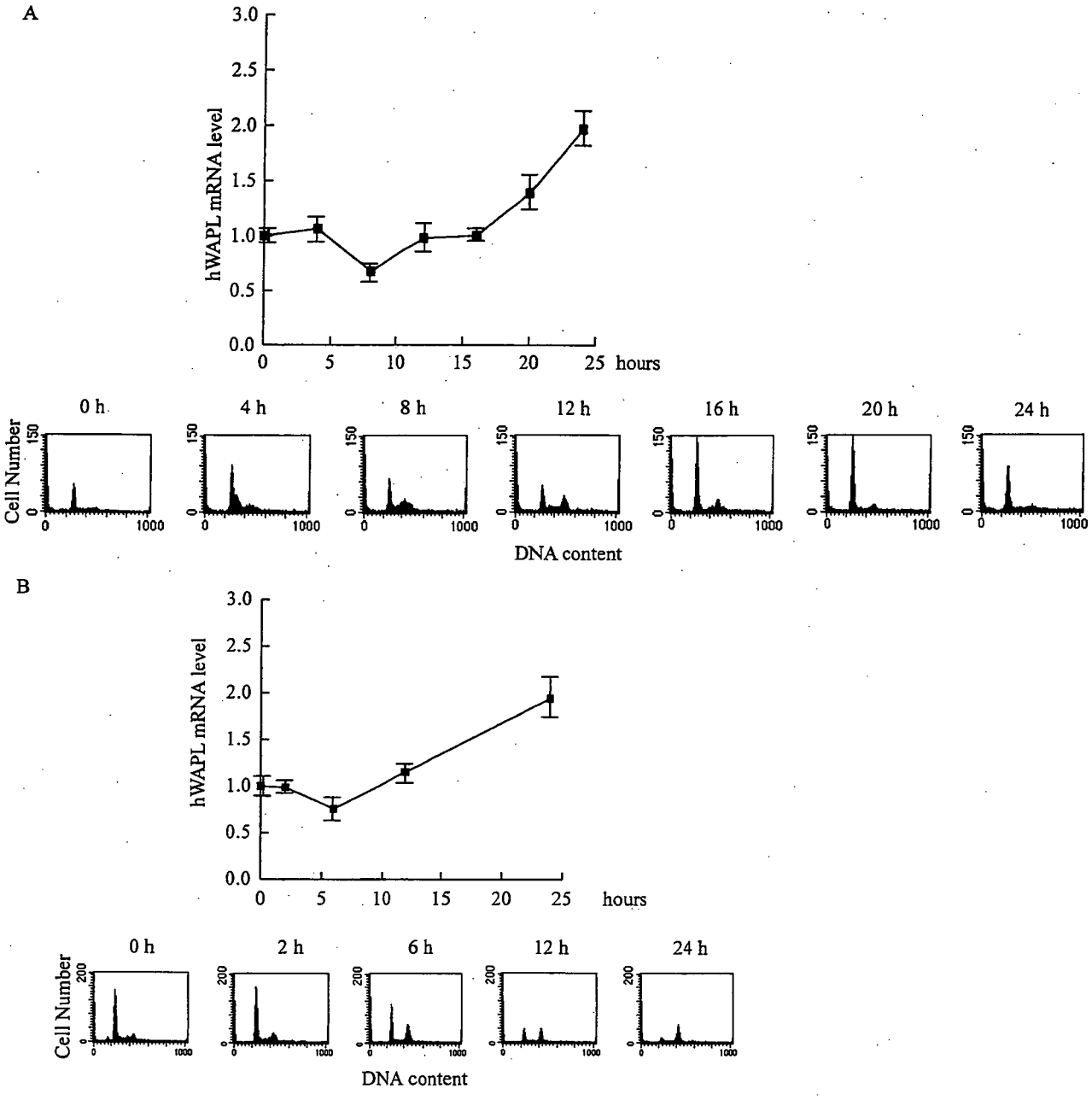

Fig. 3. Cell cycle profiles and *hWAPL* mRNA levels. *hWAPL* mRNA levels in the cells were determined by real time PCR analysis. Data were normalized to the mRNA level at 0 h that was arbitrarily set to 1 in the graphical presentation. *Bars, s.e.*. Cell cycle profiles of the cells at each time points were also confirmed by flow cytometric analysis. (A) Kinetics of *hWAPL* mRNA levels in SiHa cells at 0, 4, 8, 12, 16, 20 and 24 h after releasing from G1 arrest by 1 μg/ml aphidicolin treatment. (B) Kinetics of *hWAPL* mRNA levels in SiHa cells at 0, 2, 6, 12 and 24 h after 50 ng/ml nocodazole treatment.

3. Results and discussion

To examine whether 3-MC affects *hWAPL* expression, we treated various human uterine cervical cancer-derived cell lines with dimethylsulfoxide (DMSO) alone or 3-MC for 6 h. Then, we calculated the amounts of the *hWAPL* mRNAs in the cells by quantitative real time PCR analysis, and found that *hWAPL* mRNA levels were increased in the 3-MC-treated cells (Fig. 1A). The increases in *hWAPL* mRNA levels in SiHa cells was most remarkable among the cell lines examined. Because the *CYP1A1* gene is

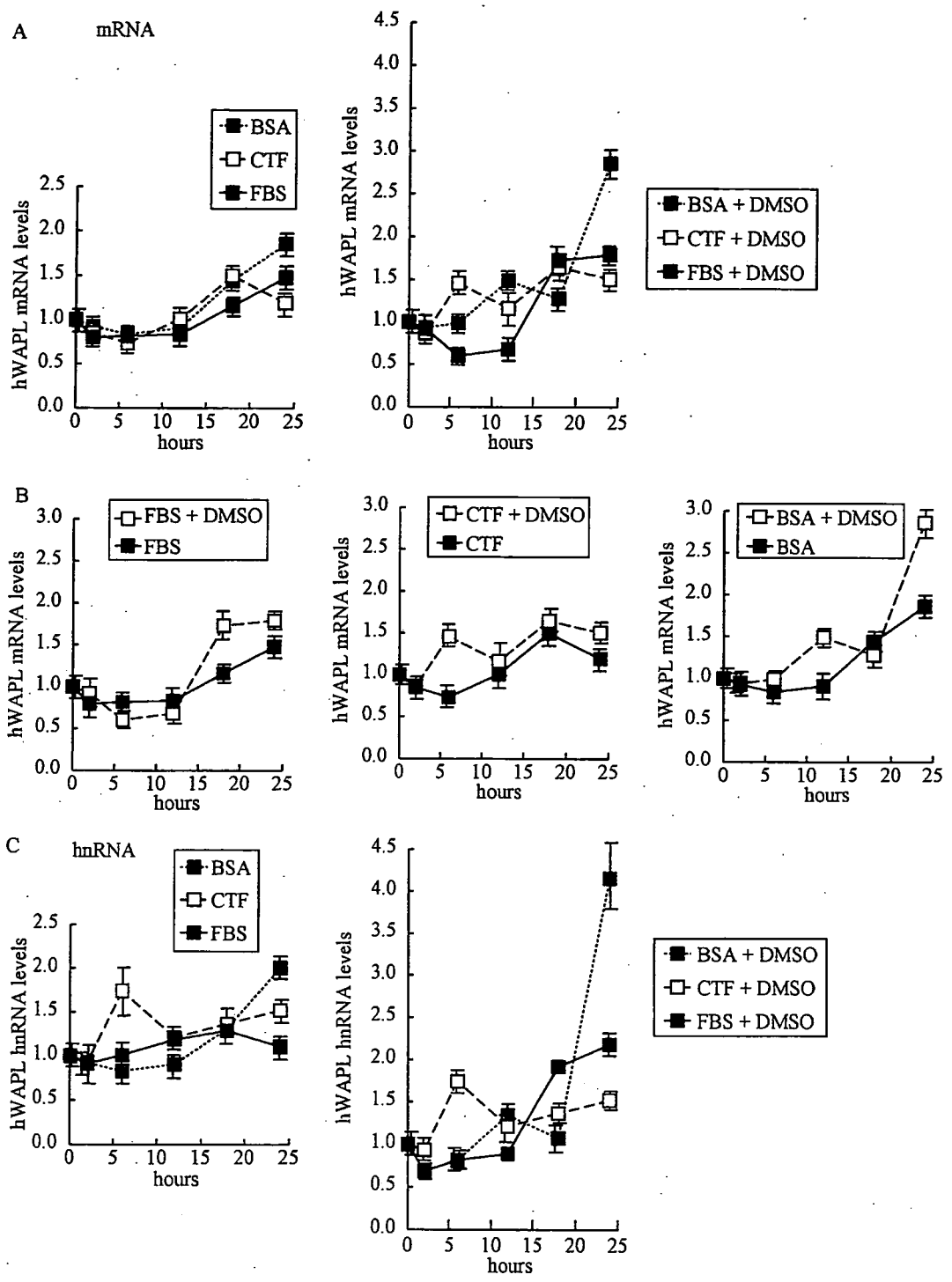

Fig. 4. Effects of FBS, CTF, BSA and DMSO on *hWAPL* mRNA and hnRNA levels in SiHa cells. *hWAPL* mRNA and hnRNA levels in SiHa cells at 0, 2, 6, 12, 18 and 24 h after replacing the growth medium to a fresh medium supplemented with FBS, CTF or BSA with or without 0.1% DMSO were deteremined by real time PCR analysis. Data were normalized to the mRNA and hnRNA level at 0 h that was arbitrarily set to 1 in the graphical presentation. *Bars, s.e.* (A) Kinetics of the *hWAPL* mRNA levels in the cells grown in the growth medium supplemented as indicated. (B) Graphical representation of the effects of DMSO on the kinetics of *hWAPL* mRNA levels in the cells grown in the growth medium supplemented with FBS, CTF or BSA. (C) Kinetics of the *hWAPL* hnRNA levels in the cells grown in the growth medium supplemented as indicated.

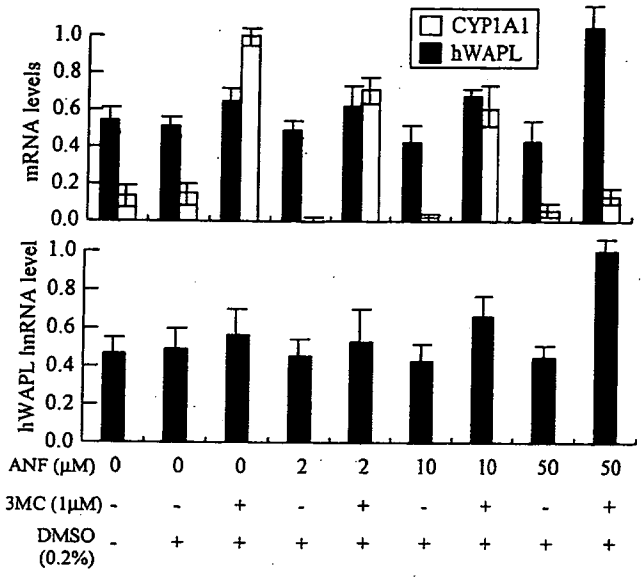

Fig. 5. Effects of AhR inhibition by α-naphthoflavone on *hWAPL* mRNA and hnRNA levels in SiHa cells treated with 3-MC. SiHa cells were treated with 0.2% DMSO alone or 1 μM 3-MC with 0. 2, 10 or 50 μM ANF for 6 h. Then, the *hWAPL* mRNA and hnRNA levels and the *CYP1A1* mRNA levels were deteremined by real time PCR analysis. SiHa cells grown for 6 h in a normal fresh medium without chemicals were also analyzed as a normal control. Data were normalized to the maximaum mRNA and hnRNA levels that were arbitrarily set to 1 in the graphical presentation. *Bars, s.e.*

a well-known target of 3-MC [12,13], we also calculated *CYP1A1* mRNA levels in the three cell lines to confirm the effects of 3-MC on the cells (Fig. 1A). We found that *CYP1A1* mRNA levels in SiHa cells were highest and increased most remarkable. *CYP1A1* mRNA in CaSki cells was not detected in our experiments. We also observed that hWAPL protein level was increased in the 3-MC-treated SiHa cells (Fig. 1B).

We next examined the effects of 3-MC on *hWAPL* expression in SiHa cells at several time points after 3-MC treatment (Fig. 2). The 3-MC-treated cells showed higher levels of *hWAPL* mRNA than the control cells at all time points examined. Interestingly, the *hWAPL* mRNA levels decreased first 6 h and then increased after changing the medium to a fresh medium containing DMSO with or without 3-MC as seen in Fig. 2.

These results prompted us to investigate whether the *hWAPL* expression is related to the cell cycle. First, to synchronize cell cycle progression, we treated SiHa cells with aphidicolin, an inhibitor of DNA synthesis, for 12 h to induce G1-phase arrest. We then released the cells from G1 arrest by changing the culture medium to a fresh growth medium. The synchronized cells were harvested every 4 h for 24 h after release from aphidicolin, and the *hWAPL* mRNA levels were calculated by quantitative real time PCR analysis (Fig. 3A). As seen in Fig. 3A, *hWAPL* mRNA initially decreased and then increased over time. Flow cytometric analysis confirmed the cell cycle phase of the cells at each time point (Fig. 3A). From these results, *hWAPL* mRNA level seemed to fluctuate in accordance with cell cycle profile. However, the levels of *hWAPL* mRNA in the cells treated with nocodazole, an inhibitor of spindle assembly, fluctuated in a similar manner to the aphidicolin-synchronized cells (Fig. 3B). Thus, amounts of *hWAPL* mRNAs are likely to have no relation to the cell cycle profiles. Recently, Guigal et al. demonstrated that FBS induces transcription of the *CYP1A1* gene. Therefore, we suspected that the fluctuation of *hWAPL* mRNA levels might be associated with the culture medium change.

To investigate the effects of components in FBS on the fluctuation of *hWAPL* mRNA levels, we examined the *hWAPL* mRNA levels in SiHa cells after changing growth medium to a fresh medium supplemented with charcoal/dextran treated FBS (CTF) or BSA instead of FBS. The fluctuations of the *hWAPL* mRNA levels showed similar trends among the cells grown with FBS, CTF and BSA (Fig. 4A; left panel). However, all cells examined in Figs. 1–3 were grown in the medium containing DMSO. Thus, we also tested the effects of DMSO with FBS, CTF or BSA at the same time. Interestingly, fluctuations of the *hWAPL* mRNA levels in SiHa cells treated with 0.1% DMSO showed different trends among FBS, CTF and BSA (Fig. 4A; right panel), and the *hWAPL* mRNA levels in the DMSO-treated cells fluctuated more drastically than that in the cells grown without DMSO (Fig. 4B). Especially, remarkable decrease of *hWAPL* mRNA levels for first 6 h after the medium change was distinctive for the growth medium supplemented with FBS and DMSO. These results suggest that DMSO and some constituents of FBS affect *hWAPL* mRNA accumulation synergistically.

mRNA levels do not always reflect on the transcription activity of genes. To investigate the kinetics of the promoter activities of the *hWAPL* gene in the cells, we evaluated the levels of *hWAPL* heterogeneous nuclear RNA (hnRNA), the unprocessed precursor of the mature and functional mRNA,

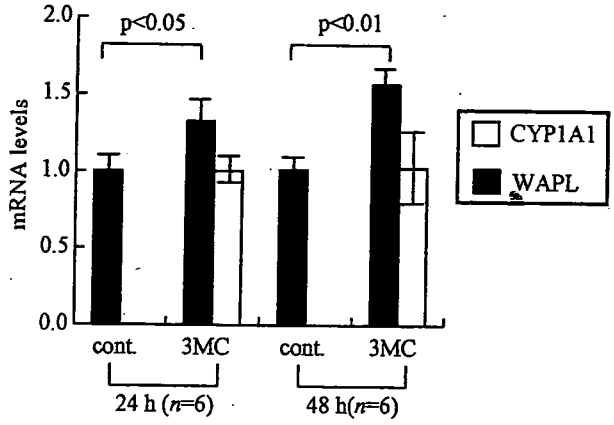

Fig. 6. Effects of 3-MC on *WAPL* mRNA levels in mouse uteri. The mice received a single intraperitoneal injection of 1 ml of olive oil containing 3-MC (3-MC) or olive oil only (cont.), and *WAPL* mRNA levels in the uteri at 24 and 48 h after injection were determined with quantitative real time PCR analysis. *CYP1A1* mRNA levels were also deteremined to confirm the effects of 3-MC on mouse uteri. The data represent the means of multiple samples normalized to the mean values of the *hWAPL* mRNA levels in the cont. 24 h samples and *CYP1A1* mRNA levels in the 3-MC 24 h samples, respectively, that were arbitrarily set to 1 in the graphical presentation. *Bars, s.e.*

by real time PCR using intron-specific primers for *hWAPL* searched in Ensembl Genome Browser (http://www.ensembl.org/). Levels of hnRNA have been proposed as a surrogate for nuclear run-on assays to determine gene transcription rates [14,15]. Although the *hWAPL* hnRNA levels fluctuated in somewhat different manner to the mRNA levels in the cells grown without DMSO, the *hWAPL* hnRNA levels in the DMSO-treated cells fluctuated in similar manner to the mRNA levels (Fig. 4C; compare with Fig. 4A). These results suggest that DMSO and some components of FBS affect transcriptional activity of the *hWAPL* gene. Increase of *hWAPL* transcription levels at 24 h in common with the cells under various conditions may be caused by the accumulation of wastes in their growth medium.

3-MC is known to be an agonist of AhR [16]. Thus, to investigate whether AhR is related to *hWAPL* transcription activation, we examined the effects of α-naphthoflavone (ANF), an AhR antagonist [17], at a dose of 2, 10 and 50 μM on *hWAPL* mRNA and hnRNA levels in 3-MC-treated SiHa cells by quantitative real time PCR analysis (Fig. 5). We also evaluated *CYP1A1* mRNA levels for monitoring the inhibitory effects on AhR functions by ANF, and found that 50 μM of ANF strongly inhibited AhR functions (Fig. 5; upper panel). Interestingly, increase of *hWAPL* mRNA levels by 3-MC was more remarkable in AhR-inhibited cells rather than that in AhR-functioning normal cells. Induction of *hWAPL* hnRNA levels showed similar manner to the *hWAPL* mRNA (Fig. 5; lower panel). From these results, we hypothesized that AhR was involved in the transcriptional regulation of *hWAPL*, but there are complex mechanisms for the transcriptional regulation of *hWAPL*. We did not find XRE motif in 5000 bp of 5′-upstream sequence of the *hWAPL* gene using MOTIF Sequence Motif Search (http://motif.genome.jp/) at the cut off score 85. Thus, although further investigation is required, we suppose that *hWAPL* is not a direct target of 3-MC but a down stream molecule of a 3-MC-targeted molecule.

Finally, we examined whether the mRNA level of a mouse homolog of *hWAPL* is increased by 3-MC in mouse uterus. Twenty-four and 48 h after the injection of 3-MC into the abdominal cavities of C57/BL6 female mice, we harvested the uteri and analyzed the *WAPL* mRNA levels by quantitative real time PCR analysis. The *CYP1A1* mRNA levels were also analyzed to confirm the 3-MC effects on the uteri. The uteri exhibited increases in *WAPL* mRNA levels compared with that of control mice (Fig. 6). These data suggest that 3-MC exposure affects *WAPL* expression in uterus.

Our recent data demonstrated that the unscheduled increase of *hWAPL* expression in human uterine cervix is associated with cervical cancer [1]. In Addition, previous studies demonstrated that 3-MC induces carcinogenesis in mouse uterine cervix [18, 19]. Thus, although the *hWAPL* induction by 3-MC was weak in our experiments, our results suggest that the promotion of carcinogenesis by 3-MC in uterus is likely to involve the *hWAPL* oncogene.

Acknowledgements

This work was supported by a Grant-in-Aid for scientific research on Priority Area (C) from the Ministry of Education, Science, Sports and Culture, and a grant from Core Research for Evolutional Science and Technology (CREST), Japan Science and Technology Corporation.

References

[1] K. Oikawa, T. Ohbayashi, T. Kiyono, H. Nishi, K. Isaka, A. Umezawa, et al., Expression of a novel human gene, human wings apart-like (hWAPL), is associated with cervical carcinogenesis and tumor progression, Cancer Res. 64 (2004) 3545–3549.

[2] F. Verni, R. Gandhi, M.L. Goldberg, M. Gatti, Genetic and molecular analysis of wings apart-like (wapl), a gene controlling heterochromatin organization in *Drosophila melanogaster*, Genetics 154 (2000) 1693–1710.

[3] K.W. Dobie, C.D. Kennedy, V.M. Velasco, T.L. McGrath, J. Weko, R.W. Patterson, G.H. Karpen, Identification of chromosome inheritance modifiers in *Drosophila melanogaster*, Genetics 157 (2001) 1623–1637.

[4] S. Reynaud, C. Duchiron, P. Deschaux, 3-Methylcholanthrene increases phorbol 12-myristate 13-acetate-induced respiratory burst activity and intracellular calcium levels in common carp (Cyprinus carpio L) macrophages, Toxicol. Appl. Pharmacol. 175 (2001) 1–9.

[5] J. Mimura, Y. Fujii-Kuriyama, Functional role of AhR in the expression of toxic effects by TCDD, Biochim. Biophys. Acta 1619 (2003) 263–268.

[6] K. Sogawa, Y. Fujii-Kuriyama, Ah receptor, a novel ligand-activated transcription factor, J. Biochem. (Tokyo) 122 (1997) 1075–1079.

[7] K. Oikawa, T. Ohbayashi, J. Mimura, R. Iwata, A. Kameta, K. Evine, et al., Dioxin suppresses the checkpoint protein, MAD2, by an aryl hydrocarbon receptor-independent pathway, Cancer Res. 61 (2001) 5707–5709.

[8] S.R. Kondraganti, P. Fernandez-Saluguero, F.J. Gonzalez, K.S. Ramos, W. Jiang, B. Moorthy, Polycyclic aromatic hydrocarbon-inducible DNA adducts: evidence by 32P-postlabeling and use of knockout mice for Ah receptor-independent mechanisms of metabolic activation in vivo, Int. J. Cancer 103 (2003) 5–11.

[9] K. Oikawa, T. Ohbayashi, J. Mimura, Y. Fujii-Kuriyama, S. Teshima, K. Rokutan, et al., Dioxin stimulates synthesis and secretion of IgE-dependent histamine-releasing factor, Biochem. Biophys. Res. Commun. 290 (2002) 984–987.

[10] M. Kuroda, T. Ishida, M. Takanashi, M. Satoh, R. Machinami, T. Watanabe, Oncogenic transformation and inhibition of adipocytic conversion of preadipocytes by TLS/FUS-CHOP type II chimeric protein, Am. J. Pathol. 151 (1997) 735–744.

[11] K. Oikawa, Y. Kosugi, T. Ohbayashi, A. Kameta, K. Isaka, M. Takayama, et al., Increased expression of IgE-dependent histamine-releasing factor in endometriotic implants, J. Pathol. 199 (2003) 318–323.

[12] N. Guigal, E. Seree, V. Bourgarel-Rey, Y. Barra, Induction of CYP1A1 by serum independent of AhR pathway, Biochem. Biophys. Res. Commun. 267 (2000) 572–576.

[13] N. Guigal, E. Seree, Q.B. Nguyen, B. Charvet, A. Desobry, Y. Barra, Serum induces a transcriptional activation of CYP1A1 gene in HepG2 independently of the AhR pathway, Life Sci. 68 (2001) 2141–2150.

[14] C.J. Elferink, J.J. Reiners Jr., Quantitative RT-PCR on CYP1A1 heterogeneous nuclear RNA: a surrogate for the in vitro transcription run-on assay, Biotechniques 20 (1996) 470–477.

[15] R.F. Johnson, C.M. Mitchell, W.B. Giles, W.A. Walters, T. Zakar, The in vivo control of prostaglandin H synthase-2 messenger ribonucleic acid expression in the human amnion at parturition, J. Clin. Endocrinol. Metab. 87 (2002) 2816–2823.

[16] M. Naruse, Y. Ishihara, S. Miyagawa-Tomita, A. Koyama, H. Hagiwara, 3-Methylcholanthrene, which binds to the arylhydrocarbon receptor, inhibits proliferation and differentiation of osteoblasts in vitro and ossification in vivo, Endocrinology 143 (2002) 3575–3581.

[17] T.A. Gasiewicz, G. Rucci, Alpha-naphthoflavone acts as an antagonist of 2,3,7, 8-tetrachlorodibenzo-p-dioxin by forming an inactive complex with the Ah receptor, Mol. Pharmacol. 40 (1991) 607–612.

[18] P. Das, A.R. Rao, P.N. Srivastava, Influence of ascorbic acid on MCA-induced carcinogenesis in the uterine cervix of mice, Cancer Lett. 72 (1993) 121–125.

[19] S. Gagandeep, S. Dhanalakshmi, E. Mendiz, A.R. Rao, R.K. Kale, Chemopreventive effects of Cuminum cyminum in chemically induced forestomach and uterine cervix tumors in murine model systems, Nutr. Cancer 47 (2003) 171–180.

J Bone Miner Metab (2005) 23:123–133
DOI 10.1007/s00774-004-0550-y

ORIGINAL ARTICLE

**Nobuyuki Kawashima · Kentaro Shindo · Kei Sakamoto
Hisatomo Kondo · Akihiro Umezawa · Shohei Kasugai
Bernard Perbal · Hideaki Suda · Minoru Takagi
Ken-ichi Katsube**

Molecular and cell biological properties of mouse osteogenic mesenchymal progenitor cells, Kusa

Received: March 15, 2004 / Accepted: September 9, 2004

Abstract A cell line of murine osteogenic progenitor cells, Kusa, was established from femoral bone marrow stromal cells with other types of mesenchymal progenitor cells. We characterized two sublines of Kusa (Kusa-A1 and Kusa-O) from several aspects, including the use of an expression profiling system, a cDNA microarray. The original Kusa subline (Kusa-A1) had high alkaline phosphatase activity and high accumulation of calcium deposits in a condition inducing mineralization, with ascorbic acid and β-glycerophosphate. Kusa-O, a low osteogenic subline of Kusa, had high alkaline phosphatase activity but slow accumulation of calcium deposits even in the inducing condition. These two Kusa sublines differed in the expression of the osteogenic marker genes, *osteocalcin* and *osteopontin*, during mineralization. A type of cDNA microarray revealed marked downregulation of gene expression in the inducing condition in both Kusa-A1 and Kusa-O. Another type of high-throughput microarray was performed to examine the difference in gene expression patterns between Kusa-A1 and Kusa-O. By this analysis, *periostin*, which would be involved in a stage of osteogenesis, was low in Kusa-A1. On the contrary, *Myocyte enhancer factor 2C (MEF2C)*, a myogenic transcriptional factor, was high in Kusa-A1, although no expression of any other myogenic genes was shown.

Key words Osteogenesis · Stem cells · Notch · MEF2 · Periostin

N. Kawashima (✉) · K. Shindo · H. Suda
Pulp Biology and Endodontics, Graduate School of Tokyo Medical and Dental University, 1-5-45 Yushima, Bunkyo-ku, Tokyo 113-8549, Japan
Tel./Fax +81-3-5803-5494
e-mail: kawashima.n.endo@tmd.ac.jp

N. Kawashima
Center of Excellence Program for Research on Molecular Destruction and Reconstruction of Tooth and Bone, Graduate School of Tokyo Medical and Dental University, Tokyo, Japan

A. Umezawa
Department of Reproductive Biology and Pathology, National Institute for Child Health and Development, Tokyo, Japan

B. Perbal
Laboratorie d'Oncologie Virale et Moléculaire, UFR de Biochimie, Université Paris, Paris, France

K. Sakamoto · M. Takagi · K. Katsube
Molecular Pathology, Graduate School of Tokyo Medical and Dental University, Tokyo, Japan

H. Kondo · S. Kasugai
Masticatory Function Control, Graduate School of Tokyo Medical and Dental University, Tokyo, Japan

N. Kawashima and K. Katsube contributed equally to this work

Introduction

The ability of mesenchymal progenitor cells to differentiate has been the subject of a growing body of documents that have revealed the unexpected potential of bone marrow cells [1,2]. Bone marrow stromal cells support the growth and differentiation of hematopoietic stem cells by both direct and indirect influences [3], and they themselves can differentiate into various types of cells, i.e., striated muscle [4], heart muscle [5], bone tissue [6], chondroctytes [7], and even neurons [8] or hepatocytes [9]. However, few studies have been done about the molecular basis of their potential, and this potential is a puzzle, considering their paradoxical stability (cells that have pluripotency but keep the quiescent state in situ) [7,10]. Further more, bone marrow progenitor cells were demonstrated to be involved in the recovery of blood vessel injury, although they caused atherosclerosis [11]. Thus, it seems that mesenchymal progenitor cells sometimes generate pathogenic change, and it is necessary to investigate their activity from a non-restitutive aspect.

The factors that regulate the potential of mesenchymal progenitor cells have been investigated in various ways. Among them, myogenesis was well-examined at a molecular level, using C3H10T1/2, a murine pluripotent fibroblastic cell line. The discovery of *MyoD* was a turning point in myogenesis research [12] and the *MyoD* gene family is now believed to control the major path of myogenesis [13].

Adipogenesis was also investigated using the same cell line, and *peroxisome proliferator-activated receptor gamma (PPAR gamma)*, a receptor of prostaglandin, was demonstrated to control the adipogenesis [14]. Compared with these investigations of myogenesis, little is known about osteogenesis and chondrogenesis. In 1997, a member of the RUNX family, CBFA1 (RUNX2) was demonstrated to be involved in osteogenesis, in a study of a null mutant mouse [15]. Recently, a type of zinc finger protein, called "osterix", was also reported to be involved in osteogenesis [16]. But the commitment of these transcriptional factors was not enough to initiate osteogenesis. Some other factors seem to be involved, but systematic investigation has not yet been done. One of the reasons might be that the cells used for such studies, e.g., primary cultures of osteoblasts or osteosarcoma cell lines, had inadequate capacity for bone formation [17,18].

Umezawa et al. [6] in experiments attempting the immortalization of murine bone marrow stromal cells, succeeded in the establishment of several mesenchymal progenitor cell lines (KUMs). One of them, named "Kusa", was unique in that it had osteogenesis potential in vivo. We investigated this cell line from the molecular aspect, including the use of cDNA microarray, to analyze the global dynamics of its gene expression pattern (gene profiling) [1,19].

Materials and methods

Cell culture

Kusa was established from mouse bone marrow stromal cells. Briefly, eluted stromal cells from the femoral bone marrow were transferred to a Dexter-type long-term culture [6]. Limiting dilution and continuous passage were performed to isolate the monoclonal cell populations. Various types of cell line were identified (KUMs) and one of them, named "Kusa", was found to possess osteoblastic properties in vivo. Five independent sublines were established from the in vivo cell mass of Kusa, after in vitro culture with limiting dilution. One of them, Kusa-A1, was selected for its particularly high osteogenic activity, and another subline, Kusa-O, was identified as non-osteogenic, although it had high alkaline phosphatase (ALP) activity. Kusa-A1 and Kusa-O were cultured in α-modified minimum essential medium containing 10% fetal calf serum. Cells were inoculated at 5000 cells/cm^2 and incubated until confluency for passage. Mineralization was induced by adding 0.2 mM ascorbic acid and 5 mM β-glycerophosphate to the same medium after confluency (inducing condition) [20,21].

Measurement of alkaline phosphatase (ALP) activity and calcium content

Alkaline phosphatase (ALP) activity was measured with an ALP measurement kit, (ALP-K Test, Wako Chemicals, Tokyo, Japan). The accumulation of calcium deposits was measured with a calcium measuring kit, Ca-E Test (Wako Chemicals), using the cell extracts treated with HCl. To determine these two activities in the cell population, normalization was performed by measuring the protein concentration in extracts. The protein concentration was measured with a DC Protein assay kit (Bio-Rad, Hercules, CA, USA). All measurements were performed by independent triplicate studies.

Northern blot and reverse transcription-quantitative reverse transcription (RT)-quantitative polymerase chain reaction (qPCR) analysis

Total RNA was extracted and purified with TRIzol (Invitrogen, Carlsbad, CA, USA). Ten micrograms of total RNA was applied to each lane of 1.2% formaldehyde agarose gel and electrophoresed. The RNA was transferred to a Nylon membrane (HybondN+; Amersham Biosciences, Piscataway, NJ, USA) and hybridized to ^{32}P-labeled DNA probes. Signals were detected and measured with a digital image analyzer, BAS-2500 (Fuji Photo Film, Tokyo, Japan). Labeled cDNA probes were made using a 488-bp fragment of mouse *Osteocalcin* (*OC*) cDNA (provided by J. Wozney [Celeste et al. [22]), a 984-bp fragment of mouse *Osteopontin* (*OPN*) cDNA (provided by Nomura et al. [23]), a 2673-bp fragment of mouse *Notch1* intracellular domain cDNA (provided by J. Nye), a 1609-bp fragment of rat *HES1* cDNA (provided by R. Kageyama), and a 2380-bp fragment of mouse *CCN3 nephroblastoma overexpressed gene (Nov)*, cloned by B. Perbal. The qPCR was performed (DyNAmo, DNA engine Opticon; MJ Japan, Tokyo, Japan) with the first-strand cDNA synthesized from 500 ng of total RNA (SuperScript II; Invitrogen). The primer sequences were as follows: MEF2C (141 bp): 5′-ATGGA TGAGCGTAACAGACAGGTG-3′ and 5′-CGTTGTAC TCGGTGTACTTGAGCA-3′; periostin (100 bp): 5′-ACC CTGCAAATGCCAACAGT-3′ and 5′-AGAATTTGCT GGAGGGCACA-3′; and βactin (380 bp): 5′-TCGGTCA GGATCTTCATGAG-3′ and 5′-AGTACCCCATTGAA CATGGC-3′.

cDNA array analysis

Global examination of gene expression was performed with a cDNA gene expression array (Atlas mouse cDNA Expression Array; BD Biosciences Clontech, Palo Alto, CA, USA). This microarray carries 588 mouse cDNAs for general profiling. The complete list of cDNAs is available at the website of Clontech (http://www.clontech.com). The extracted total RNA was eluted through an oligo-dT cellulose (Amersham Sciences, Piscataway, NJ, USA) column to purify polyA mRNA. cDNA probes were made from the poly A mRNA, following the manufacturer's protocol, with the specific primers and [α-^{32}P] dATP and hybridized to the array membrane. Signals were detected and measured with a digital image analyzer (BAS-2500).

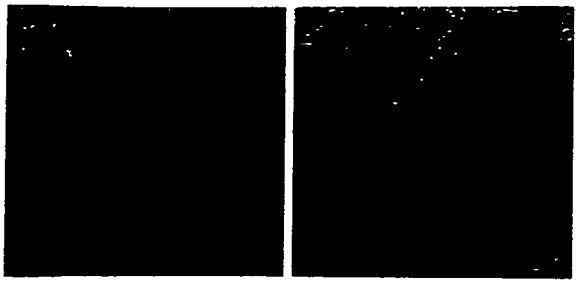

Fig. 1. Phase contact photomicrographs of Kusa-A1 and Kusa-O. Morphologically, Kusa-A1 (**A**) and Kusa-O (**B**) were similar, with a spindle or polygonal shape. Kusa-O was slightly larger than Kusa-A1 in cell size. *Bar* represents 100μm

Another microarray analysis was done with the GEMarray (Incyte/Genome Systems, Palo Alto, CA, USA). This microarray was based on a fluorescence labeled (Cy3 and Cy5) cDNA probe to distinguish the two sources. Hybridization on the slide glasses and image analysis were done by the company. The results were expressed in reference to the GenBank addresses.

Results

Morphological properties of Kusa

Before confluence, Kusa-A1 had a fibroblastic appearance, with a polygonal flat or spindle shape (Fig. 1A). Kusa-O was slightly larger than Kusa-A1 in cell size (Fig. 1B), although no significant difference was observed. Kusa did not exhibit tumor-cell-like growth, such as piling up, nor did it form a focus in normal medium (non-inducing condition). On treatment with ascorbic acid and β-glycerophosphate (inducing condition), Kusa-A1 exhibited mineralization (Fig. 2). Kusa-A1 gradually accumulated extracellular matrices as small sandy precipitates that covered the surface of cell aggregates. The accumulation was positively stained with Alizarin Red S. These nodules were visible on day 3 and showed condensed staining on day 5 (Fig. 2B,C). In the non-inducing condition, Kusa-A1 spontaneously exhibited nodule-like structures on day 5, although the nodules were rather small and not stained with Alizarin Red S (Fig. 2A). Kusa-O did not exhibit rapid mineralization. In the inducing condition, mineralized nodules were gradually accumulated from day 10 (Fig. 2E,F,G). The Alizarin Red S-positive spots in Kusa-O were rather large but diffuse, and their margins were not clear, as compared with the nodule margins in Kusa-A1. In the non-inducing condition, Kusa-O formed nodules, but they were rather small and not stained with Alizarin Red S (Fig. 2D). High magnification of the Kusa-A1 culture stained with Alizarin Red S showed that the calcified area appeared like "spots", distinctly separate from the non-calcified area (Fig. 2H). The calcified area in Kusa-O showed obscure margins and non-condensed stain (Fig. 2I).

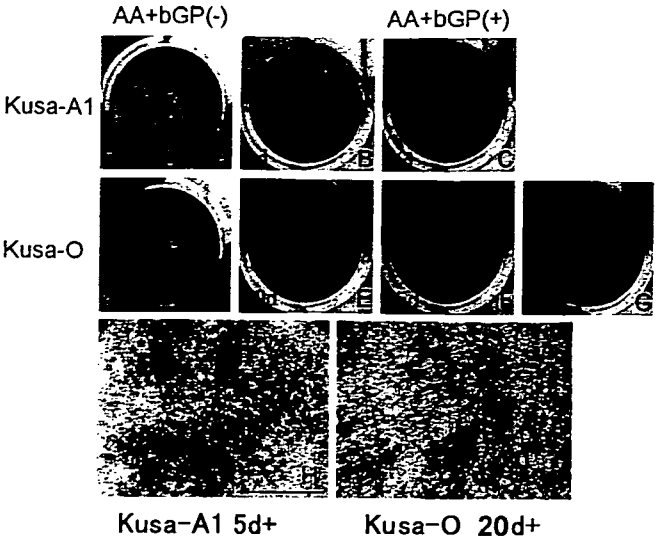

Fig. 2. Mineralized nodule formation in *Kusa-A1* and *Kusa-O*. Mineralized nodules were detected by Alizarin Red S staining. Kusa-A1 cultured in the non-inducing condition (without ascorbic acid [*AA*] and β-glycerophosphate [β*GP; AA* + β*GP*(−)] did not form mineralized nodules 5 days (*d*) after confluency (**A**), but in the inducing condition (addition of AA and β*GP AA* + β*GP*(+)) these nodules were formed on day 3 (**B**), and nodules showing condensed staining were formed on day 5 (**C**). Kusa-O did not form mineralized nodules 20 days after confluency in the non-inducing condition (**D**), but, in the inducing condition, formed them on day 10 (**E**); the nodules then developed moderately (**F** day 15; **G** day 20). **H** and **I** show high-magnification views of mineralized nodules. **H** In Kusa-A1, the nodules had a discrete margin (*asterisks* indicating the development of "salt-and-pepper pattern"-like dot structures, but in Kusa-O (**I**), the margins of the nodules were ambiguous. *Bar* represents 500μm. **A–G** ×1

Calcium accumulation

Kusa-A1 and Kusa-O apparently differed in calcium accumulation rates (Fig. 3). In the non-inducing condition, neither Kusa-A1 nor Kusa-O exhibited calcium accumulation until day 5. However, Kusa-A1 showed marked accumulation of calcium deposits in the inducing condition. On day 5, the calcium level was 20-fold higher than that in the initial state. Kusa-O was not reactive to the inducing condition and showed little change even on day 5. MC3T3-E1 cells (a mouse osteoblastic cell line) did not show apparent accumulation of calcium deposits during the time course.

ALP activity and insoluble calcium content

Kusa-A1 had extraordinarily high ALP activity (0.8IU/mg) even before mineralization, and this activity was constant both in the inducing and the non-inducing conditions (Fig. 3). The very high ALP activity of Kusa-A1 was marked as compared with that in MC3T3-E1, which had 20-fold less ALP activity than Kusa-A1. Kusa-O had relatively low ALP activity at the beginning (though it was much higher than that in MC3T3-E1), but the activity gradually increased in the inducing condition, to 1.2IU/mg on day 5.

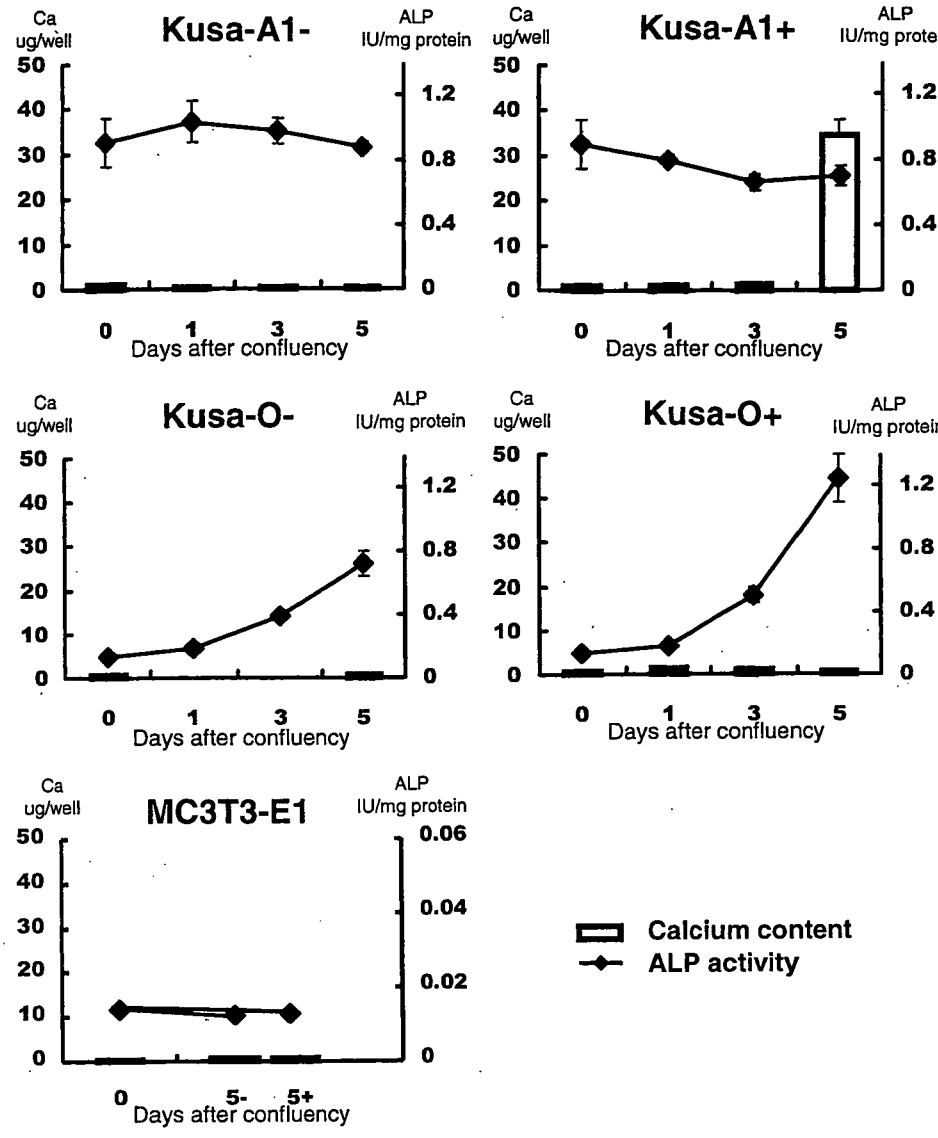

Fig. 3. Calcium accumulation and alkaline phosphatase (*ALP*) activity in Kusa-A1 and Kusa-O Calcium accumulation was observed only in Kusa-A1 on day 5 after confluency in the inducing condition (*Kusa-A1+*). High ALP activity was observed in Kusa-A1 in the non-inducing condition (*Kusa-A1−*) and ALP was rather low in the inducing condition (Kusa-A1+). ALP activity in Kusa-O was not high at the beginning, but was gradually upregulated during the time course in the non-inducing condition (*Kusa-O−*) and the inducing condition accelerated this upregulation (*Kusa-O+*). ALP activity in *MC3T3-E1* was much lower than that in Kusa-A1 and Kusa-O. MC3T3-E1 was cultured in both inducing and non-inducing conditions. *Minus sign* "−" indicates the absence of AA and βGP and "+" indicates the presence of AA and βGP

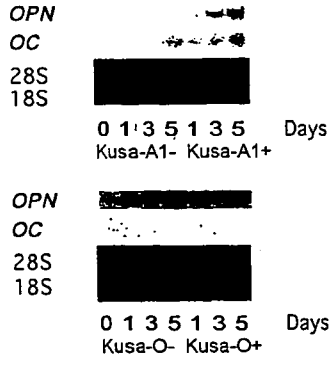

Fig. 4. *Osteocalcin* (*OC*) and Osteopontin (*OPN*) expression in Kusa-A1 and Kusa-O. In Kusa-A1, *Osteocalcin* expression was observed on day 5 in the non-inducing condition, and was seen on day 1 in the inducing condition. Its expression was gradually upregulated in the time course. In contrast, Kusa-O did not express *Osteocalcin*. *Osteopontin* expression was high only in the inducing condition in Kusa-A1, but its expression was observed in both conditions in Kusa-O. *Minus sign* "(−)" indicates the absence of AA and βGP and + indicates the presence of AA and βGP

Expression of osteogenic marker genes

We examined two osteogenic markers, *osteopontin* (*OPN*) and *osteocalcin* (*OC*) (Fig. 4). In Kusa-A1, *osteopontin* expression was not detectable in the non-inducing condition, although *Osteocalcin* was slightly upregulated. In the inducing condition, *osteocalcin* expression was high from day 1 and gradually increased. *Osteopontin* expression was gradually upregulated in the inducing condition. Kusa-O showed a relatively constant level of *osteopontin* expression in the inducing condition, whereas the level was high in the non-inducing condition. *Osteocalcin* expression was not detectable in Kusa-O in either the inducing or the non-inducing condition.

Expression of Notch signal genes

To examine the properties of Kusa as stem cells, genes related to the Notch signal were investigated (Fig. 5). The

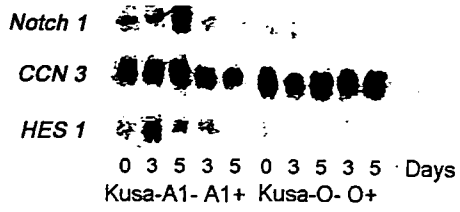

Fig. 5. Notch signal expression in *Kusa-A1* and *Kusa-O*. *Top row, Notch1; middle row, CCN3 (Nov); bottom row, HES1. Minus sign* (−) indicates the absence of AA and βGP and + indicates the presence of AA and βGP

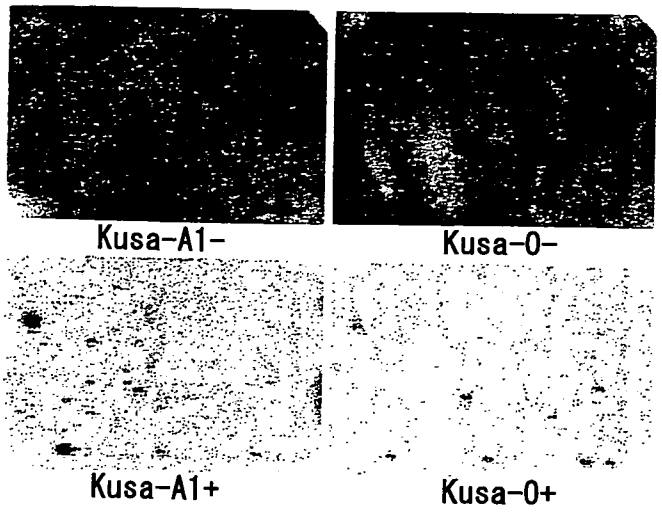

Fig. 6. Atlas Microarray (Clontech) surveillance of Kusa-A1 and Kusa-O in both the non-inducing and the inducing conditions. The profile of Kusa-A1 was generally similar to that of Kusa-O. The inducing condition showed a marked downregulation of gene expression in both cell lines. *Minus sign* (−) indicates the absence of AA and βGP and + indicates the presence of AA and βGP

Notch signal is fundamental for the regulation of stem cells, and *CCN3* is a regulator of the Notch signal whose expression is often found in mesenchymal cells. *CCN3* expression was discrete in both Kusa-A1 and Kusa-O. In Kusa-A1, it was high in the non-inducing condition. *Notch1* expression in Kusa-A1 was observed in the non-inducing condition. Weak *Notch1* expression was observed on day 3 in the inducing condition in both Kusa-A1 and Kusa-O. *HES1* expression in Kusa-A1 was transiently upregulated in the non-inducing condition. In Kusa-O, *HES1* expression was not observed. In conclusion, subtle differences were observed in the expression patterns of the examined genes related to the Notch signal.

Gene expression profile, using cDNA microarray

To clarify the differences in gene expression in Kusa-A1 and Kusa-O in detail, global examination was done using microarray methods. We performed cDNA array analysis of 588 genes with the Atlas Mouse cDNA Expression Array (Clontech) (Fig. 6) in both the inducing and non-inducing conditions. From an overview of the hybridization image, it was clear that global downregulation occurred in the inducing condition in both Kusa-A1 and Kusa-O. In the non-inducing condition, about 140 genes were expressed in the panel, and in the inducing condition, about 50 genes (including several housekeeping genes) were expressed. In about 50 remaining genes, no genes directly involved in osteogenesis were found (Table 1). However, several genes possibly related to osteogenesis (Table 1) showed differences between the cell lines. For Kusa-A1, *ski* and *TIMP 2* and *3* were upregulated in the inducing condition. In contrast, *MAPKK1* and *TGFβ2* were upregulated for Kusa-O.

To compare the expression patterns between Kusa-A1 and Kusa-O, another type of microarray, (GEMarray; Incite/Genome Systems) was carried out, which could analyze more than 8000 clones. Several genes (clones) that showed great differences in expression were demonstrated (Tables 2 and 3) though they did not include known genes directly related to osteogenesis. Tables 2 and 3 show that *myocyte enhancer factor 2C (MEF2C)* is a gene that was highly expressed in Kusa-A1. This gene is regulated principally by other myogenic transcriptional factors, such as MyoD and Myf5, but the GEMarray analysis did not show upregulation of any other myogenic markers. The expression rate of *MEF2C* was also confirmed by qRT-PCR (Fig. 7). In contrast to the expression of *MEF2C* in Kusa-O, *periostin* (also known as *osteblast-specific factor-2 [OSF-2]*) was high in Kusa-O (Fig. 7). The role of this fasciclin 1-like extracellular protein has not yet been clarified, but it may play a role in the recruitment and attachment of osteoblast precursors in the periosteum [24].

Discussion

We investigated the properties of an osteogenic cell line, Kusa, from several aspects. This cell line has unidirectional potential for osteogenesis/mineralization in the normal condition and was classified into two sublines, Kusa-A1 and Kusa-O, by mineralization activity. Kusa-A1 had high ability for osteogenesis/mineralization in vivo and in vitro. The osteogenic ability of Kusa-A1 was remarkable; it showed mineralization within 5 days in the inducing condition, whereas a well-known mouse osteoblastic cell line, MC3T3-E1, first demonstrated mineralized nodules only on day 20 (personal data). Kusa-O was relatively slow to show mineralization as compared with Kusa-A1, but it is not appropriate to call it "non-osteogenic", because its activity was almost the same as that of MC3T3-E1. Both Kusa sublines should be categorized as high osteogenic cell lines.

The high ALP activity of Kusa was remarkable when compared with that of the osteogenic cell line MC3T3-E1. The constant high ALP activity in Kusa-A1 may have influenced its strong mineralization ability, and the progressive upregulation of ALP in Kusa-O would explain its slow mineralization. Calcium deposition was faster in Kusa-A1 than in Kusa-O in the inducing condition, but in the

Table 1. Atlas mouse cDNA expression array (Clontech) results

Experimental		Control
A1−	*VS*	O−

	Spot Intensity							
Coordinate	O−	A1−	Ratio	Difference	UP	DOWN	Gene	Genbank no.
D4k	0	7830	N/C	−7830	UP		Interferon inducible protein 1	U19119
D3l	194	5724	29.51	−5530	UP		HMG-box transcription factor from testis (MusSox17)	D49474
F7n	1312	12118	9.24	−10806	UP		Tissue inhibitor of metalloproteinases 3 (TIMP3); SUN	L19622
F7m	1538	7758	5.04	−6220	UP		Tissue inhibitor of metalloproteinases 2 (TIMP2)	X62622
C3h	2237	10392	4.65	−8155	UP		FLICE-like inhibitory protein long form (FLIP-L)	U97076
A4g	1301	5912	4.54	−4611	UP		Ski protooncogene	U14173
A7m	20965	12092	0.58	8873		DOWN	Prothymosin alpha (PTMA)	X56135
B1b	8176	4402	0.54	3774		DOWN	HSP60	X53584
B1d	11509	5186	0.45	6323		DOWN	HSP86; heat shock 86-kDa protein	M36830
F4g	11315	5012	0.44	6303		DOWN	Transforming growth factor beta 2 precursor (TGF-beta 2)	X57413
A1c	6224	2730	0.44	3494		DOWN	Breast cancer type 2 susceptibility protein (BRCA2)	U65594
C1m	7286	3096	0.42	4190		DOWN	Glutathione reductase	X76341
F7a	12115	4714	0.39	7401		DOWN	Interleukin-converting enzyme (ICE)	L28095
B6a	13899	4406	0.32	9493		DOWN	MAP kinase kinase 1	L02526

Experimental		Control
A1+	*VS*	A1−

	Spot Intensity							
Coordinate	A1−	A1+	Ratio	Difference	UP	DOWN	Gene	Genbank no.
A1g	9784	997	9.81	−8787		DOWN	Mothers against dpp protein 1 (msMAD1; mSMAD1; MADH1); TGF-beta signaling protein 1 (BSP1)	U58992
B4a	8622	890	9.69	−7732		DOWN	NF-kappa-B transcription factor p65 subunit (NF-κB p65); relA; NFKB3	M61909
E3d	12134	1415	8.58	−10719		DOWN	Interleukin-3 receptor	M29855
E3h	5924	1014	5.84	−4910		DOWN	Interleukin-8 receptor	D17630
F3k	9742	1860	5.24	−7882		DOWN	7S Nerve growth factor alpha subunit (alpha-NGF; NGFA); KLK4	M11434

F7l	12804	2914	4.39	−9890		DOWN	47-kDa Heat shock protein precursor (HSP47); collagen-binding protein 1 (CBP1); serine protease inhibitor J6	J05609
E3f	23780	6790	3.50	−16990		DOWN	Interleukin-5 receptor alpha subunit precursor (IL-5R alpha)	D90205
C3h	10392	3185	3.26	−7207		DOWN	FLICE-like inhibitory protein long form (FLIP-L)	U97076
D3l	6392	2700	2.37	−3692		DOWN	HMG-box transcription factor from testis (MusSox17)	D49474
F7n	12118	5446	2.23	−6672		DOWN	Tissue inhibitor of metalloproteinases 3 (TIMP3); SUN	L19622
B5i	1182	4778	0.25	3596	UP		58-kDa Inhibitor of RNA-activated protein kinase	U28423
D6h	1500	7089	0.21	5589	UP		T-Lymphocyte activated protein	M31042
C2e	424	4561	0.09	4137	UP		Tumor necrosis factor alpha-induced protein 3 (TNFAIP3; TNFIP3); A20 zinc finger protein	U19463

Experimental		Control
O+	*VS*	O−

Spot intensity

Coordinate	O−	O+	Ratio	Difference	UP	DOWN	Gene	Genbank no.
D5m	8545	0	N/C	−8545		DOWN	Split hand/foot gene	U41626
D6n	7025	0	N/C	−7025		DOWN	cAMP-Dependent transcription factor 3 (ATF3); activating factor 3; transcription factor LRG-21	U19118
D6m	5215	0	N/C	−5215		DOWN	Transcription factor LIM-1	Z27410
B1d	7205	864	8.34	−6341		DOWN	HSP86; heat shock 86-kDa protein	M36830
B4a	5790	874	6.62	−4916		DOWN	NF-kappa-B transcription factor p65 subunit (NF-κB p65); relA; NFKB3	M61909
F7l	6700	2020	3.32	−4680		DOWN	47-kDa Heat shock protein precursor (HSP47); collagen-binding protein 1 (CBP1); serine protease inhibitor J6	J05609
B6a	8700	2786	3.12	−5914		DOWN	Dual-specificity mitogen-activated protein kinase kinase 1 (MAP kinase kinase 1; MAPK kinase 1; MAPKK1); erk activator kinase 1 (MEK1); PRKMK1	L02526
F7a	7584	2460	3.08	−5124		DOWN	Interleukin-converting enzyme (ICE)	L28095
D1n	1628	9729	0.17	8101	UP		Sim transcription factor	U42554
B5i	1182	7497	0.16	6315	UP		58-kDa Inhibitor of RNA-activated protein kinase	U28423
F7d	1093	8084	0.14	6991	UP		Protease nexin 1 (PN-1)	X70296
D6m	0	8331	0.00	8331	UP		Transcription factor LIM-1	Z27410

The ratio of each pair was calculated with signal intensity, and if the ratio was more than 1.67 or less than 0.6, the spotted genes were considered to be upregulated or downregulated, respectively
Minus sign (−) indicates the absence of AA and βGP and (+) indicates the presence of AA and βGP

Table 2. Mouse GEM array (Incite/Genome Systems) results: sorted by balanced differential expression in descending order

Differential expression	Kusa-A1 signal	Kusa-O signal	Gene name
5.1	18153	3573	Tissue inhibitor of metalloproteinase 3 (IMAGE:580753)
4.4	2254	516	Myocyte enhancer factor 2C (IMAGE:777101)
3.8	6829	1778	Alkaline phosphatase 2, liver (IMAGE:535409)
3.6	1963	542	ESTs (IMAGE:735883)
3.3	12133	3631	Tenascin C (IMAGE:736372)
3.3	803	241	*Mus musculus* neural precursor cell expressed developmentally; downregulated Nedd9 (Nedd9) mRNA, complete cds (IMAGE:404536)
2.9	15184	5181	Procollagen, type V, alpha 2 (IMAGE:467107)
2.8	8897	3222	Procollagen, type V, alpha 2 (IMAGE:445075)
2.6	1071	409	ESTs (IMAGE:597280)
2.5	3927	1544	ESTs (IMAGE:419146)
2.5	1683	667	ESTs (IMAGE:479709)[a]
2.4	5265	2152	Procollagen, type XI, alpha 1 (IMAGE:423028)
2.4	2616	1069	Public domain EST (IMAGE:597342)
2.3	6241	2702	Public domain EST (IMAGE:439362)
2.3	1737	749	Kinesin family member 5B (IMAGE:760837)
2.3	829	362	*Mus musculus* major histocompatibility complex region NG27, NG28, RPS28, NADH oxidoreductase, NG29, KIFC1, Fas-binding protein, BING1, tapasin, RalGDS-like, KE2, BING4, beta 1,3-galactosyl transferase, and RPS18 genes, complete cds (IMAGE:329741)
2.3	2778	1226	Sprouty homolog 1 (Drosophila) (IMAGE:425005)
2.2	2866	1314	ESTs (IMAGE:466255)
2.2	2214	1006	ESTs, weakly similar to plexin 1 (*M.musculus*) (IMAGE:735903)
2.2	1339	609	Adducin 3 (gamma) (IMAGE:620815)
2.2	5249	2434	Alkaline phosphatase 2, liver (IMAGE:465052)

[a] IMAGE:479709 clone was similar to *Mus musculus* MADS box transcription enhancer factor 2, polypeptide C (myocyte enhancer factor 2C)

Table 3. Mouse GEM array (Incyte/Genome Systems) results: sorted by balanced differential expression in ascending order

Differential expression	Kusa-A1 signal	Kusa-O signal	Gene name
−5.3	951	5080	Stromal cell-derived factor 1 (IMAGE:533003)
−4.5	205	929	ESTs (IMAGE:779168)
−4.5	156	708	ESTs, weakly similar to cDNA EST EMBL:D75506 comes from this gene (*C.elegans*) (IMAGE:334182)
−4.4	220	963	ESTs (IMAGE:445426)
−4	1303	5260	Secreted phosphoprotein 1 (IMAGE:571759)
−3.9	362	1408	Four and a half LIM domains 1 (IMAGE:477066)
−3.7	456	1671	Fibrillin 2 (IMAGE:617885)
−3.7	218	809	Complement component 1, r subcomponent (IMAGE:617816)
−3.6	830	3021	Mus musculus OSF-2/periostin mRNA, complete cds (IMAGE:403071)[a]
−3.4	1204	4149	ESTs (IMAGE:617992)
−3.3	324	1060	Complement component 1 subcomponent (IMAGE:676176)
−3	507	1535	Calpain 6 (IMAGE:478504)
−2.9	812	2315	*Mus musculus* mRNA for dickkopf-3 (dkk-3 gene) (IMAGE:536577)
−2.8	1076	3010	Phosphodiesterase 7A (IMAGE:314384)
−2.8	366	1007	Public domain EST (IMAGE:314509)
−2.7	731	1939	ESTs (IMAGE:536526)
−2.6	1044	2672	Chloride channel 2 (IMAGE:407704)
−2.6	291	768	ESTs, weakly similar to proline-rich protein MP4 (*M.musculus*) (IMAGE:458992)
−2.6	274	708	Insulin-like growth factor 1 (IMAGE:313322)
−2.5	2177	5462	ESTs, weakly similar to similarity to yeast D-lactate dehydrogenase (*C.elegans*) (IMAGE:748228)
−2.5	280	693	Public domain EST (IMAGE:479159)
−2.4	2279	5428	Procollagen, type VI, alpha 1 (IMAGE:334132)
−2.4	992	2350	ESTs, highly similar to hypothetical 25.7-kD protein in MSH1-EPT1 intergenic region (*Saccharomyces cerevisiae*) (IMAGE:337654)
−2.4	329	787	Public domain EST (IMAGE:338162)

[a] Periostin, originally called OSF-2 (fasciclin I-like), is mainly detected in the periosteum and may play a role in the recruitment and attachment of osteoblast precursors (22)

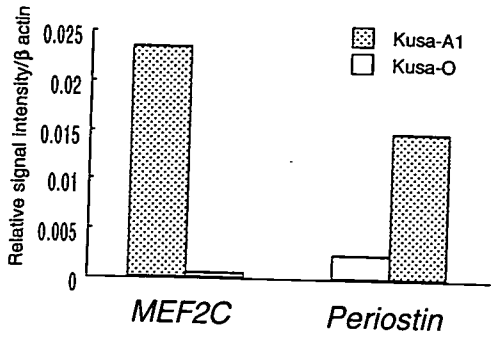

Fig. 7. *MEF2C* and *Periostin* expression in Kusa-A1 (*gray bars*) and Kusa-O (*white bars*). Reverse transcription-quantitative polymerase chain reaction (RT-qPCR) confirmed the data obtained by microarray (Table 2). In Kusa-A1, *MEF2C* was highly expressed, but *Periostin* expression was low. On the other hand, in Kusa-O, *MEF2C* expression was low, but *Periostin* expression was high

non-inducing condition, neither of these cell lines exhibited calcium deposits. These results imply that the recruitment of inorganic phosphate by ALP is a necessary but not sufficient condition to induce calcium deposition.

The differential expression of the osteogenic markers, *osteocalcin* and *osteopontin*, in Kusa-A1 and Kusa-O indicates their stage of osteogenesis. Osteocalcin, a kind of bone "gla" (gamma carboxy-glutamic acid) protein (BGP), is the major non-collagenous extracellular protein of bone tissue, and is thought to play an important role in bone mineral deposition with its gamma caboxy-glutamic acid residues [25]. *Osteopontin* is another osteogenic marker expressed in the middle stage of osteoblast differentiation in vitro. In this study, Kusa-A1 showed osteocalcin expression within 1 day after confluency in the inducing condition and 5 days after confluency in the non-inducing condition. But Kusa-O did not exhibit osteocalcin expression in either the inducing condition or the inducing condition. On the other hand, *osteopontin* expression was rather constant through the experimental time course in Kusa-O, but was high only in the inducing condition in Kusa-A1. To summarize these results, Kusa-A1 could be classified as a more mature stage of osteoblast than Kusa-O, a classification which is compatible with their osteogenesis/mineralization abilities in vivo and in vitro.

For Kusa-A1, some specific conditions have induced its differentiation into various types of cells. For example, Makino et al. [5] showed that Kusa-A1 differentiated into adipocytes or myotubes with 5-aza cytidine treatment. Moreover, the introduction of noggin, a suppressor of bone morphogenic protein (BMP) induced active neurons from Kusa-A1 [8]. These results indicate that Kusa should be considered as a kind of stem cell or progenitor cell, not as a simple osteoblastic cell line. We examined the expression of Notch signal-related genes that could be important for the regulation of various types of stem/progenitor cells. Notch signaling in stem cells models is often demonstrated as lateral inhibition or lateral specification [26,27]. These models well explain the "salt-and-pepper pattern" seen in the differentiation of stem cells [28], in which an active Notch signal creates reciprocal patterns in neighboring cells. Our high-magnification view of calcified deposits in Kusa-A1 indicated this salt-and-pepper-like pattern, which may correspond to an activated Notch signal. In contrast, the obscure pattern of calcification in Kusa-O may indicate an inactive state of Notch signaling. In fact, our previous study demonstrated that a constitutively active form of Notch1 influenced the osteogenesis/mineralization ability of Kusa [29]. But Northern blot analysis showed that *HES1*, a downstream gene in the Notch signal pathway, changed its expression level only in Kusa-A1, in the non-inducing condition. The Notch signal has many different downstream factors, such as nuclear factor kappaB, p-300, Deltex, and mitogen-activated protein kinase (MAPK), other than the Epstein-Barr virus (EBV) latency C promoter binding factor 1 (CBF1)/hairy and enhancer of split 1 (HES1) pathway and employs them differentially. *HES1* may not be involved in the Notch signal pathway of Kusa.

Actually, the analysis of 588 cDNAs is not sufficient to use the term "global", but, with this small-number microarray, we detected that gross downregulation occurred in the inducing condition in both Kusa-A1 and Kusa-O. This indicates that "master gene expression" is not necessarily associated with osteogenesis/mineralization in Kusa, and conversely, the gross downregulation may carve out specific networks of signal pathways, resulting in the unidirectional differentiation of osteogenesis/mineralization. This hypothesis is a concept that is completely opposite to the "master gene theory", and further verification with other types of cell lines should be performed to test this hypothesis.

The high-throughput microarray (GEMarray), which was carried on Kusa-A1 and Kusa-O in the non-inducing condition, revealed a relatively high expression of *periostin* in Kusa-O cells. Periostin was identified from the screening of MC3T3-E1-specific genes, and sequence similarity analysis has revealed that it is homologous to fasciclin [30], a type of homophilic binding molecule [31,32]. Periostin is specifically expressed in the periosteum and the periodontal ligament [24]. The function of periostin remains to be elucidated, but recent reports indicate a relationship with cell attachment [33–36]. As compared with Kusa-A1, MC3T3-E1 in the non-inducing condition should be classified as showing a rather immature state of osteogenesis, and Kusa-O should also be included in this category. The high level of expression of *periostin* in MC3T3-E1 and Kusa-O may imply its role in the early stage of osteogenesis, although further investigation remains to be done to specify the molecular basis of this role.

In contrast to *periostin* expression in Kusa-A1, *MEF2C* showed enhanced expression. *MEF2C* is a basic/helix-loop-helix (bHLH) transcriptional factor and is known to be a late-stage regulator of myogenesis, under the control of *MyoD*, *Myf5*, and some other early myogenic genes [37–39]. However, we could not find upregulation of any other myogenic genes with the GEMarray microarray analysis. Recently, further roles and relationships of *MEF2C* have been found, such its action as an apoptotic factor in neurogenesis [40,41] and stem cell regulation, in the context of Notch

signaling, in both vertebrates and invertebrates [42]. As mentioned, it was difficult to find the direct involvement of *HES1* in the Notch pathway of Kusa, though activation of the Notch signal has been shown to suppress the differentiation of Kusa-A1 [29]. The Notch signal seems to employ some pathway(s) other than its classical one, and *MEF2C* could be a candidate. *CCN3* is a positive regulator of the Notch signal and its high expression in Kusa may be related to this kind of non-classical pathway of the Notch signal.

In conclusion, we investigated two sublines of Kusa from several different aspects and clarified their specific characteristics. Kusa seems to be a useful cell line, considering its high osteogenesis/mineralization activity; investigation of the molecular basis of this activity will give new insights for the technical development of osteogenic restitution.

Acknowledgments This work was supported by Grants-in-Aids from the Japanese Society for the Promotion of Science: no. 14370615 to N.K; and nos. 15390552 and 12671763 to K.K.

References

1. Gershon D (2002) Microarray technology: an array of opportunities. Nature 416:885–891
2. Pittenger MF, Mackay AM, Beck SC, Jaiswal RK, Douglas R, Mosca JD, Moorman MA, Simonetti DW, Craig S, Marshak DR (1999) Multilineage potential of adult human mesenchymal stem cells. Science 284:143–147
3. Dexter TM, Testa NG (1976) Differentiation and proliferation of hemopoietic cells in culture. Methods Cell Biol 14:387–405
4. Seale P, Rudnicki MA (2000) A new look at the origin, function, and "stem-cell" status of muscle satellite cells. Dev Biol 218:115–124
5. Makino S, Fukuda K, Miyoshi S, Konishi F, Kodama H, Pan J, Sano M, Takahashi T, Hori S, Abe H, Hata J, Umezawa A, Ogawa S (1999) Cardiomyocytes can be generated from marrow stromal cells in vitro. J Clin Invest 103:697–705
6. Umezawa A, Maruyama T, Segawa K, Shadduck RK, Waheed A, Hata J (1992) Multipotent marrow stromal cell line is able to induce hematopoiesis in vivo. J Cell Physiol 151:197–205
7. Hall FL, Han B, Kundu RK, Yee A, Nimni ME, Gordon EM (2001) Phenotypic differentiation of TGF-beta1-responsive pluripotent premesenchymal prehematopoietic progenitor (P4 stem) cells from murine bone marrow. J Hematother Stem Cell Res 10:261–271
8. Kohyama J, Abe H, Shimazaki T, Koizumi A, Nakashima K, Gojo S, Taga T, Okano H, Hata J, Umezawa A (2001) Brain from bone: efficient "meta-differentiation" of marrow stroma-derived mature osteoblasts to neurons with Noggin or a demethylating agent. Differentiation 68:235–244
9. Mitaka T (2001) Hepatic stem cells: from bone marrow cells to hepatocytes. Biochem Biophys Res Commun 281:1–5
10. Steidl U, Kronenwett R, Rohr UP, Fenk R, Kliszewski S, Maercker C, Neubert P, Aivado M, Koch J, Modlich O, Bojar H, Gattermann N, Haas R (2002) Gene expression profiling identifies significant differences between the molecular phenotypes of bone marrow-derived and circulating human CD34+ hematopoietic stem cells. Blood 99:2037–2044
11. Sata M, Saiura A, Kunisato A, Tojo A, Okada S, Tokuhisa T, Hirai H, Makuuchi M, Hirata Y, Nagai R (2002) Hematopoietic stem cells differentiate into vascular cells that participate in the pathogenesis of atherosclerosis. Nat Med 8:403–409
12. Lassar AB, Paterson BM, Weintraub H (1986) Transfection of a DNA locus that mediates the conversion of 10T1/2 fibroblasts to myoblasts. Cell 47:649–656
13. Weintraub H, Davis R, Tapscott S, Thayer M, Krause M, Benezra R, Blackwell TK, Turner D, Rupp R, Hollenberg S, Zhuang Y, Lassar A (1991) The myoD gene family: nodal point during specification of the muscle cell lineage. Science 251:761–766
14. Tontonoz P, Hu E, Spiegelman BM (1994) Stimulation of adipogenesis in fibroblasts by PPAR gamma 2, a lipid-activated transcription factor. Cell 79:1147–1156
15. Komori T, Yagi H, Nomura S, Yamaguchi A, Sasaki K, Deguchi K, Shimizu Y, Bronson RT, Gao YH, Inada M, Sato M, Okamoto R, Kitamura Y, Yoshiki S, Kishimoto T (1997) Targeted disruption of Cbfa1 results in a complete lack of bone formation owing to maturational arrest of osteoblasts. Cell 89:755–764
16. Nakashima K, Zhou X, Kunkel G, Zhang Z, Deng JM, Behringer RR, de Crombrugghe B (2002) The novel zinc finger-containing transcription factor osterix is required for osteoblast differentiation and bone formation. Cell 108:17–29
17. Rodan GA, Noda M (1991) Gene expression in osteoblastic cells. Crit Rev Eukaryot Gene Expr 1:85–98
18. Yasui N, Ochi T, Takaoka K, Ono K, Nakata Y (1980) Osteogenesis by factor(s) isolated from mouse osteosarcoma cells in combination with collagen. Biken J 23:83–87
19. Chen JJ, Wu R, Yang PC, Huang JY, Sher YP, Han MH, Kao WC, Lee PJ, Chiu TF, Chang F, Chu YW, Wu CW, Peck K (1998) Profiling expression patterns and isolating differentially expressed genes by cDNA microarray system with colorimetry detection. Genomics 51:313–324
20. Ecarot-Charrier B, Glorieux FH, van der Rest M, Pereira G (1983) Osteoblasts isolated from mouse calvaria initiate matrix mineralization in culture. J Cell Biol 96:639–643
21. Schoeters GE, de Saint-Georges L, Van den Heuvel R, Vanderborght O (1988) Mineralization of adult mouse bone marrow in vitro. Cell Tissue Kinet 21:363–374
22. Celeste AJ, Rosen V, Buecker JL, Kriz R, Wang EA, Wozney JM (1986) Isolation of the human gene for bone gla protein utilizing mouse and rat cDNA clones. Embo J 5:1885–1890
23. Nomura S, Wills AJ, Edwards DR, Heath JK, Hogan BL (1988) Developmental expression of 2ar (osteopontin) and SPARC (osteonectin) RNA as revealed by in situ hybridization. J Cell Biol 106:441–450
24. Horiuchi K, Amizuka N, Takeshita S, Takamatsu H, Katsuura M, Ozawa H, Toyama Y, Bonewald LF, Kudo A (1999) Identification and characterization of a novel protein, periostin, with restricted expression to periosteum and periodontal ligament and increased expression by transforming growth factor beta. J Bone Miner Res 14:1239–1249
25. Boskey AL, Gadaleta S, Gundberg C, Doty SB, Ducy P, Karsenty G (1998) Fourier transform infrared microspectroscopic analysis of bones of osteocalcin-deficient mice provides insight into the function of osteocalcin. Bone 23:187–196
26. Sternberg PW (1988) Lateral inhibition during vulval induction in *Caenorhabditis elegans*. Nature 335:551–554
27. Freitas C, Rodrigues S, Charrier JB, Teillet MA, Palmeirim I (2001) Evidence for medial/lateral specification and positional information within the presomitic mesoderm. Development 128: 5139–5147
28. Marnellos G, Deblandre GA, Mjolsness E, Kintner C (2000) Delta-Notch lateral inhibitory patterning in the emergence of ciliated cells in Xenopus: experimental observations and a gene network model. Pac Symp Biocomput 5:329–340
29. Shindo K, Kawashima N, Sakamoto K, Yamaguchi A, Umezawa A, Takagi M, Katsube K, Suda H (2003) Osteogenic differentiation of mesenchymal progenitor cells, Kusa is suppressed by Notch signaling. Exp Cell Res 290:370–380
30. Takeshita S, Kikuno R, Tezuka K, Amann E (1993) Osteoblast-specific factor 2: cloning of a putative bone adhesion protein with homology with the insect protein fasciclin I. Biochem J 294 (Pt 1):271–278
31. Elkins T, Hortsch M, Bieber AJ, Snow PM, Goodman CS (1990) Drosophila fasciclin I is a novel homophilic adhesion molecule that along with fasciclin III can mediate cell sorting. J Cell Biol 110:1825–1832
32. Elkins T, Zinn K, McAllister L, Hoffmann FM, Goodman CS (1990) Genetic analysis of a Drosophila neural cell adhesion molecule: interaction of fasciclin I and Abelson tyrosine kinase mutations. Cell 60:565–575
33. Shao R, Bao S, Bai X, Blanchette C, Anderson RM, Dang T, Gishizky ML, Marks JR, Wang XF (2004) Acquired

expression of periostin by human breast cancers promotes tumor angiogenesis through up-regulation of vascular endothelial growth factor receptor 2 expression. Mol Cell Biol 24:3992–4003

34. Nakazawa T, Nakajima A, Seki N, Okawa A, Kato M, Moriya H, Amizuka N, Einhorn TA, Yamazaki M (2004) Gene expression of periostin in the early stage of fracture healing detected by cDNA microarray analysis. J Orthop Res 22:520–525
35. Kudo H, Amizuka N, Araki K, Inohaya K, Kudo A (2004) Zebrafish periostin is required for the adhesion of muscle fiber bundles to the myoseptum and for the differentiation of muscle fibers. Dev Biol 267:473–487
36. Bao S, Ouyang G, Bai X, Huang Z, Ma C, Liu M, Shao R, Anderson RM, Rich JN, Wang XF (2004) Periostin potently promotes metastatic growth of colon cancer by augmenting cell survival via the Akt/PKB pathway. Cancer Cell 5:329–339
37. Takebayashi-Suzuki K, Pauliks LB, Eltsefon Y, Mikawa T (2001) Purkinje fibers of the avian heart express a myogenic transcription factor program distinct from cardiac and skeletal muscle. Dev Biol 234:390–401
38. Sartorelli V, Huang J, Hamamori Y, Kedes L (1997) Molecular mechanisms of myogenic coactivation by p300: direct interaction with the activation domain of MyoD and with the MADS box of MEF2C. Mol Cell Biol 17:1010–1026
39. Edmondson DG, Lyons GE, Martin JF, Olson EN (1994) Mef2 gene expression marks the cardiac and skeletal muscle lineages during mouse embryogenesis. Development 120:1251–1263
40. Okamoto S, Krainc D, Sherman K, Lipton SA (2000) Antiapoptotic role of the p38 mitogen-activated protein kinase-myocyte enhancer factor 2 transcription factor pathway during neuronal differentiation. Proc Natl Acad Sci U S A 97:7561–7566
41. Okamoto S, Li Z, Ju C, Scholzke MN, Mathews E, Cui J, Salvesen GS, Bossy-Wetzel E, Lipton SA (2002) Dominant-interfering forms of MEF2 generated by caspase cleavage contribute to NMDA-induced neuronal apoptosis. Proc Natl Acad Sci U S A 99:3974–3979
42. Wilson-Rawls J, Molkentin JD, Black BL, Olson EN (1999) Activated notch inhibits myogenic activity of the MADS-Box transcription factor myocyte enhancer factor 2C. Mol Cell Biol 19: 2853–2862

Molecular Biology of the Cell
Vol. 16, 1491–1499, March 2005

Immortalization of Human Fetal Cells: The Life Span of Umbilical Cord Blood-derived Cells Can Be Prolonged without Manipulating p16^{INK4a}/RB Braking Pathway[D]

Masanori Terai,*† Taro Uyama,* Tadashi Sugiki,* Xiao-Kang Li,‡ Akihiro Umezawa,*§ and Tohru Kiyono†

Departments of *Reproductive Biology and Pathology and ‡Innovative Surgery, National Research Institute for Child Health and Development, Tokyo 157-8535, Japan; †Virology Division, National Cancer Center Research Institute, Tokyo, Japan; and §Department of Pathology, Keio University School of Medicine, Tokyo 160-8582, Japan

Submitted July 31, 2004; Accepted December 20, 2004
Monitoring Editor: Lawrence Goldstein

Human umbilical cord blood-derived mesenchymal stem cells (UCBMSCs) are expected to serve as an excellent alternative to bone marrow-derived human mesenchymal stem cells. However, it is difficult to study them because of their limited life span. To overcome this problem, we attempted to produce a strain of UCBMSCs with a long life span and to investigate whether the strain could maintain phenotypes in vitro. UCBMSCs were infected with retrovirus carrying the human telomerase reverse transcriptase (hTERT) to prolong their life span. The UCBMSCs underwent 30 population doublings (PDs) and stopped dividing at PD 37. The UCBMSCs newly established with hTERT (UCBTERTs) proliferated for >120 PDs. The p16^{INK4a}/RB braking pathway leading to senescence can be inhibited by introduction of Bmi-1, a polycomb-group gene, and human papillomavirus type 16 E7, but the extension of the life span of the UCBMSCs with hTERT did not require inhibition of the p16^{INK4a}/RB pathway. The characteristics of the UCBTERTs remained unchanged during the prolongation of life span. UCBTERTs provide a powerful model for further study of cellular senescence and for future application to cell-based therapy by using umbilical cord blood cells.

INTRODUCTION

Human mesenchymal stem cells (hMSCs) can be a useful source of cells for transplantation for several reasons: they have the ability to proliferate and differentiate into mesodermal tissues, and they entail no ethical or immunological problems (Caplan, 1991; Prockop, 1997; Caplan and Bruder, 2001). hMSCs have been studied extensively over the past 3 decades, and numerous independent research groups have successfully isolated hMSCs from a variety of sources, most commonly, from the bone marrow (Owen, 1988; Umezawa *et al.*, 1992; Jaiswal *et al.*, 1997; Makino *et al.*, 1999; Pittenger *et al.*, 1999; Sekiya *et al.*, 2004). Umbilical cord blood (UCB) contains circulating stem/progenitor cells, and the cells contained in UCB are known to be distinct from those contained in bone marrow and adult peripheral blood (Mayani and Lansdorp, 1998). Isolation, characterization, and differentiation of clonally expanded hMSCs derived from UCB (UCBMSCs) have been reported (Goodwin *et al.*, 2001; Lee *et al.*, 2004), and UCBMSCs have been found to have multipotency, and the immunophenotype of the clonally expanded cells is consistent with that reported for bone marrow mesenchymal stem cells. Even now, most UCB is regarded as medical waste in the delivery rooms. Aspirating bone marrow from patients is, however, an invasive procedure, and the proliferation and differentiation capacity of hMSCs decreases with the donor age (D'Ippolito *et al.*, 1999). Therefore, the applications of UCB should be further expanded.

UCBMSCs will be useful sources for cell transplantation, however, it is difficult to study and apply them because of their limited life span. One of the reasons for this is that normal human cells undergo a limited number of cell division in culture and then enter a nondividing state called "senescence" (Hayflick, 1976; Campisi, 1997). Human cells reach senescence or cease to divide after a limited number of cell replications, and the average number of hMSC population doublings (PDs) has been found to be ~40 (Takeda *et al.*, 2004), implying that it would be difficult to obtain enough cells to restore the function of a failing human organ. Large numbers of cells must be injected into damaged tissues to restore function in humans, and cells sometimes need to be injected throughout entire organs.

To resolve these problems, the life span of hMSCs from bone marrow can be extended by retroviral transduction of human telomerase reverse transcriptase (hTERT) (Blackburn, 2000a,b, 2001) and human papillomavirus type 16 (HPV16) E6 and/or E7 (Sekiguchi *et al.*, 1999; Burk *et al.*, 2003; Takeda *et al.*, 2004). Both p16^{INK4a}/RB inactivation with E7 and telomerase activation with E6 are required to extend the life span of human mammary epithelial cells (Kiyono *et al.*, 1998). E6 also accelerates degradation of p53, which induces the cdk inhibitor p21 (Sekiguchi and Hunter, 1998). This system in which p16^{INK4a}/RB is inhibited and

This article was published online ahead of print in *MBC in Press* (http://www.molbiolcell.org/cgi/doi/10.1091/mbc.E04-07-0652) on January 12, 2005.

[D] The online version of this article contains supplemental material at *MBC Online* (http://www.molbiolcell.org).

Address correspondence to: Akihiro Umezawa (umezawa@1985.jukuin.keio.ac.jp).

telomerase is activated is highly efficient in extending the life span of hMSCs (Okamoto *et al.*, 2002).

In the present study, we investigated the growth regulatory mechanism of UCBMSCs and attempted to establish UCBMSCs with hTERT (UCBTERTs) to overcome their limited life span. Introduction of hTERT alone was sufficient to extend the life span of UCBMSCs in vitro, and this technique for prolonging the life span of UCBMSCs will be a useful tool. UCBTERTs with the extended life span provide a powerful model for further study of cellular senescence and application to transplantation therapy in the future.

MATERIALS AND METHODS

Isolation and Cell Culture of UCBMSCs

UCB was collected on delivery with informed consent. UCB mononuclear cells were obtained as per the manufacturer's instructions, followed by Ficoll-Paque (Amersham Biosciences, Piscataway, NJ) density gradient centrifugation (1.077 g/cm^3), and plated in tissue culture dishes (BD Biosciences, San Jose, CA) in DMEM medium (Sigma-Aldrich, St. Louis, MO) and 10% fetal bovine serum (FBS) (Vitromex, Geilenkirchen, Germany). All cultures were maintained at 37°C in a humidified atmosphere containing 95% air and 5% CO_2. A few colonies were found in the culture dish 1 mo after the collected cells were cultured in DMEM with 10% FBS. One colony was trypsinized using a colony cylinder and then diluted and plated on 12-well plates (BD Biosciences) in mesenchymal stem cell growth medium (MSCGM, PT-3001; Cambrex Bio Science Walkersville, Walkersville, MD) at a final density of ~4 × 10^5 cells/well in a 12-well plate. MSCGM was used in all culture procedures after harvesting the colony. The cells were passaged at a density of ~1 × 10^5 cells/100-mm dish (1:4), and the original cells were regarded as being PD 0 (day 0). When the cultures reached subconfluence, the cells were harvested with 0.25% trypsin and 1 mM EDTA and replated with one-half of the harvested cells. Cells were allowed to adhere overnight, and nonadherent cells were washed out with medium changes. Medium changes were carried out twice weekly thereafter. The cells were cultured for further experiments under the approval (approval nos. 7 and 55) of the Ethics Committee of National Research Institute for Child Health and Development, Tokyo.

Infection with Recombinant Retroviruses

The cells were prepared for infection with recombinant retroviruses expressing the E6, E7, and hTERT, as described previously (Takeda *et al.*, 2004). Stably transduced cells with an expanded life span were designated UCBE6E7-20 and UCBTERT-21 cells.

Senescence-associated-β-gal (SA-β-gal) Staining

The SA-β-gal assay was performed as described previously (Dimri *et al.*, 1995). Cells were washed in phosphate-buffered saline (PBS), fixed for 3–5 min at room temperature in 2% formaldehyde/0.2% glutaraldehyde (or 3% formaldehyde), washed, and incubated at 37°C with fresh SA-β-gal stain solution: 1 mg of 5-bromo-4-chloro-3-indolyl β-D-galactosidase per milliliter (stock is 20 mg of dimethylformamide/ml), 40 mM citric acid/sodium phosphate, pH 6.0, 5 mM potassium ferrocyanide, 5 mM potassium ferricyanide, 150 mM NaCl, and 2 mM $MgCl_2$. Staining was evident in 2–4 h and maximal in 12–16 h.

Cell Transplantation

Freshly collected confluent cells (10^6 cells) were subcutaneously and intramuscularly injected into BALB/c nu/nu mice (Sankyo Laboratory, Hamamatsu, Japan). Animals were monitored for malignant transformation of the injected cells for 3 mo after inoculation and then killed by cervical location.

Flow Cytometric Analysis

Cells were stained for 30 min at 4°C with primary antibodies and immunofluorescent secondary antibodies. The cells were then analyzed on a FACScan (BD Biosciences), and the data were analyzed with the CELLQUEST software (BD Biosciences). Antibodies against human CD13, CD14, CD29, CD31, CD34, CD44, CD45, CD50, CD55, CD59, CD90, CD117, and CD133 were purchased from Beckman Coulter (Fullerton, CA), Immunotech (Marseille, France), Cytotech (Hellebaek, Denmark), and BD Biosciences PharMingen (San Diego, CA).

Western Blot Analysis

Cells were seeded at a density of 3 × 10^5 cells/100-mm culture dish and harvested at subconfluence. Cell lysates were prepared by sonication by using ultrasonic homogenizer VP-5S in WE16th lysis buffer (Gewin *et al.*, 2004). Equal amounts of protein (20 μg) were loaded on SDS-polyacrylamide gels and blotted on Immobilon-P membranes (Millipore, Bedford, MA) by using a semidry transfer system (Atto, Tokyo, Japan). The primary antibodies used were as follows: G3-245 for retinoblastoma (RB) protein and G175-405 for p16^{INK4a} (BD Biosciences PharMingen), DO-1 for p53 (Oncogene Science, Cambridge, MA), F-5 for p21 and I-19 for actin (Santa Cruz Biotechnology, Santa Cruz, CA), affinity-purified anti-phospho-ataxia telangiectasia mutated kinase (p-ATM) (Ser1981) (600-401-400; Rockland, Gilbertsville, PA), and phospho-p53 (p-p53) (Ser15) antibody (9284; Cell Signaling Technology, Beverly, MA). Blots were probed with horseradish peroxidase-conjugated goat anti-mouse IgG (Jackson ImmunoResearch Laboratories, West Grove, PA), anti-rabbit IgG (New England Biolabs, Beverly, MA), or donkey anti-goat IgG (Santa Cruz Biotechnology), and visualized using an enhanced chemiluminescence detection kit (Roche Diagnostics, Indianapolis, IN).

Telomere Length Assay

Total genomic DNA was isolated from cultured cells by proteinase K digestion. The lengths of telomere in each sample were determined by Southern blot analysis as described previously (Vaziri *et al.*, 1994). Briefly, 1 μg of genomic DNA extracted from each sample was digested with both *Hinf*I and *Rsa*I and electrophoresed in 0.8% agarose gels for 16 h, transferred onto a Hybond N membrane (Amersham Biosciences), and hybridized with digoxigenin (DIG)-labeled (TTAGGG)$_3$ probe. The membrane was incubated with anti-DIG alkaline phosphatase (ALP) antibody, and detection was performed with chemiluminescence solution.

Telomerase Activity

Telomerase activity in each sample was detected by the telomeric repeat amplification protocol (TRAP) assay by using the TRAPeze kit (Intergen, Purchase, NY) according to the manufacturer's instruction.

Karyotype Analysis

Fixation and chromosome preparation were performed according to the standard procedure described previously (Sasaki, 1975). For each sample, >50 cells were scored for their chromosome number.

Differentiation-Induction Experiments

The multidirectional differentiation potential of each cell line was assessed by the differentiation-induction protocols described below.

Histochemical Staining

After 21 d of culture, cells were rinsed twice with PBS and then fixed with 10% buffered formalin for 10 min at room temperature. The fixed cells were stained with 0.3% Oil-Red-O (Nakarai Tesque, Kyoto, Japan) for the adipogenic differentiation assay and with 5% silver nitrate (Nakarai Tesque) for von Kossa staining in the osteogenic differentiation assay (Tsuchiya *et al.*, 2004).

Osteogenic Differentiation

Cells were seeded at a density of 5 × 10^4 cells/cm^2 in tissue culture dishes and cultured with MSCGM containing 100 nM dexamethasone, 50 μM ascorbic, acid 2-phosphate, and β-glycerophosphate. The cultures were maintained for 4 wk, and the cultured medium was replaced every 3 d.

Adipogenic Differentiation

Cells were seeded at a density of 3 × 10^4 cells/cm^2 in tissue culture dishes. When the cells were confluent, the adipogenic differentiation was initiated by three cycles of induction/maintenance culture. Each cycle consists of 3 d of culture in the induction medium (DMEM with 10% FBS, 1 μM dexamethasone, 0.2 mM indomethacin, 10 μg/ml insulin, and 0.5 mM 3-isobutyl-1-methylxanthine) followed by 2 d of culture in the maintenance medium (DMEM with 10% FBS and 10 μg/ml insulin).

RESULTS

Establishment of UCB-derived Cells with an Extended Life Span

UCBMSCs regarded as being PD 0, or day 0, were fibroblast-like in morphology, indistinguishable in appearance from the marrow-derived MSCs, and relatively larger in size than rapidly self-renewing stem cells (Prockop *et al.*, 2001) and multipotent adult progenitor stem cells (Jiang *et al.*, 2002) (Figure 1A). The cells from PD 9 to PD 31 rapidly proliferated in culture, and propagated continuously (Figure 1, B and C). No SA-β-gal activity was detected histoenzymologically in the UCBMSCs in the growth phase on day 59. The UCBMSCs stopped replicating, became broad and flat, and exhibited SA-β-gal activity as indicated by blue staining of

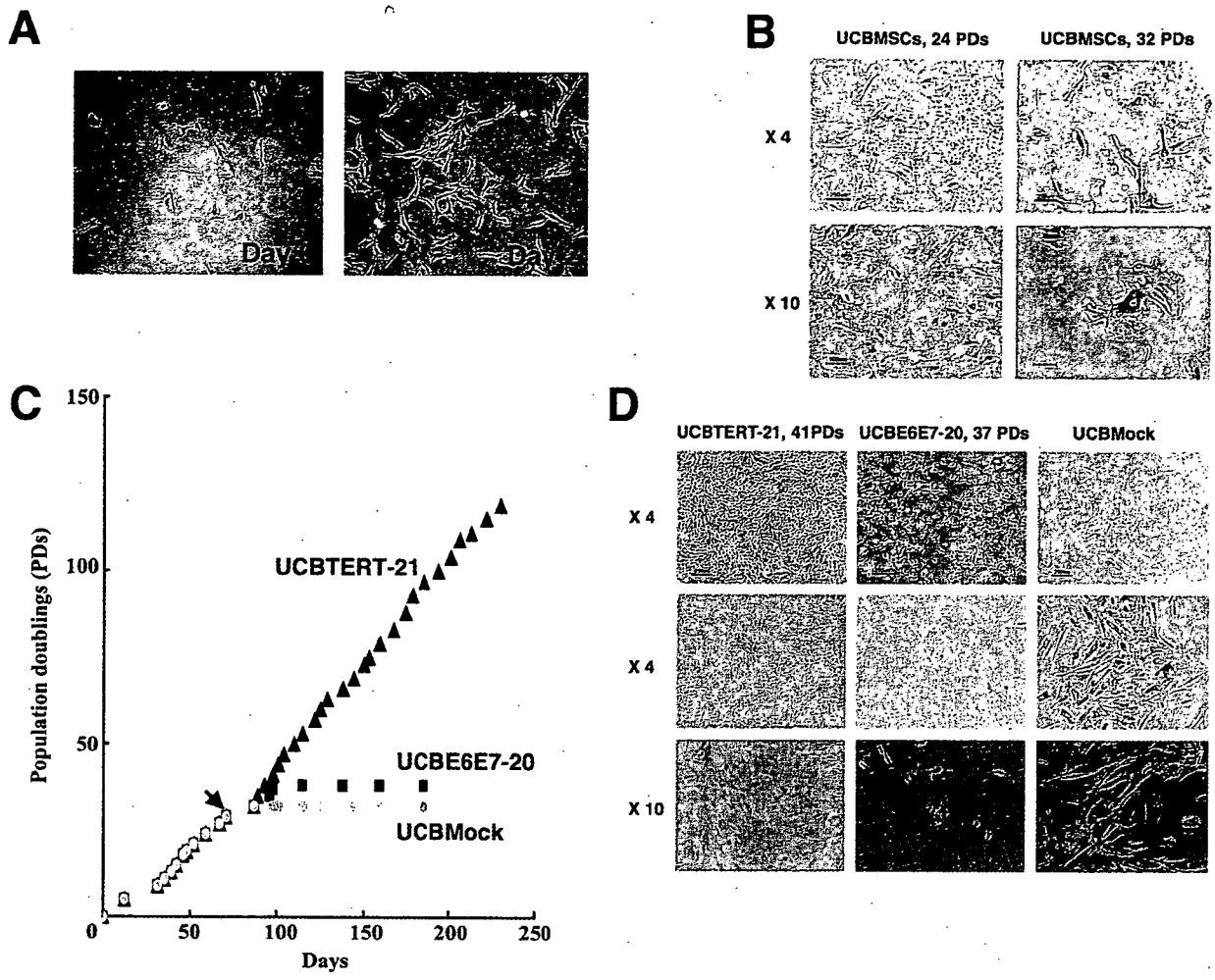

Figure 1. In vitro growth and SA-β-gal activity of UCBMSCs, UCBE6E7-20 cells, and UCBTERT-21 cells. (A) Morphology of human UCBMSCs (left, day 0; right, day 2; original magnification, 10×). (B) Morphological changes and SA-β-gal activity of UCBMSCs. UCBMSCs were a broad and flat, ceased to proliferate, and exhibited high SA-β-gal activity as indicated by their cytoplasm staining blue at PD 32 (14 passages at day 98), suggesting senescence. No SA-β-gal activity was detected in the UCBMSCs in the growth phase at PD 24 (10 passages at day 59 in left column). Bar, 250 μm in the upper column and 100 μm in the lower column. (C) Population doublings of UCBMock cells (yellow circles), UCBE6E7-20 cells (red squares), and UCBTERT-21 cells (blue triangles) are shown. UCBMSCs were infected with recombinant retroviruses carrying E6 and E7 or hTERT or were treated with polybrene alone at PD 29 (indicated as an arrow). UCBTERT-21 cells proliferated for >120 PDs and for >250 d and exhibited persistent growth. UCBE6E7-20 cells exhibited a prolonged cell life span in culture, reached 38 PDs, and then entered crisis. UCBMock cells stopped growing and entered senescence at 32 PDs. (D) Morphological changes (top column) and SA-β-gal activity (middle and bottom column) of UCBMock cells, UCBE6E7-20 cells, and UCBTERT-21 cells. No staining was detected in UCBTERT-21 cells at PD 41 (left column, 16 passages at day 98) with the SA-β-gal stain (middle and bottom columns). A few UCBE6E7 cells were positive with SA-β-gal stain at PD 37 (middle column, 15 passages at day 98). UCBMock cells were broad and flat at PD 32 (right column, 14 passage at day 98), indicating senescence.

their cytoplasm at PD 32 or day 98, indicating that they had entered senescence (Figure 1, B and C). The morphological changes and SA-β-gal activity of UCBMSCs are PD dependent. To extend the cells' life span and obtain a large number of cells, two different types of cells were obtained by transferring a combination of HPV16 E6 and E7 or hTERT at 29 PDs or 12 passages (Figure 1C, indicated as an arrow). UCBMSCs transduced with a combination of E6 and E7 were designated UCBE6E7-20 cells, and UCBMSCs transduced with hTERT were named UCBTERT-21 cells. UCBTERT-21 cells successfully proliferated >120 PDs, and continued to grow. The cells were found to have an extended life span (Figure 1C, UCBTERT-21 cells, blue triangles). The UCBE6E7-20 cells, which had been transduced with E6 and E7, had a prolonged cell life span in culture, and underwent global cell death at 38 PDs, when the cells entered a "crisis" period. This implies that the E6 and E7 are capable of prolonging cell life span but that their effect is limited (Figure 1C, UCBE6E7-20 cells, pink squares). Mock infection (polybrene treatment alone) did not extend cell life span, and the cells reached senescence or cessation of growth at PD 32 (Figure 1C, UCBMock, yellow circles). SA-β-gal staining was performed to determine the proportions of cells that had entered senescence, and positive staining was observed in 0% of the UCBTERT-21 cells at PD 41, 2% of the UCBE6E7-20 cells at PD 37, and 100% of the UCBMock cells at PD 32 (Figure 1D). The low percentage of SA-β-gal–positive UCBE6E7-20 cells at PD 37 or day 98 is probably attributable to global cell death by crisis (Figure 1D, middle column). UCBMock cells exhibited a typical senescence-associated morphology, i.e., they were broad and flat and exhibited strong SA-β-